NUMERICAL SIMULATION OF THE DEVELOPMENT OF STRESSES IN YOUNG CONCRETE

M. Cervera y E. Schaumann

Barcelona, July 2003

Contents

Chapter 1

Introduction

1.1 Motivation and Background

Quality control during construction is one of the challenges of today's engineering practice, both with regard to the loss of durability and to the functionality of the structures being built. In concrete technology, cracking is an issue of major concern, and it is primarily associated with thermal (and shrinkage) effects, specially at early ages.

Temperature-related criteria are commonly used to control the risk of cracking on site. However, practical experience proves that these criteria are often unreliable. Mangold (1994) explained in his Doctoral Thesis that an important reason for this uncertainty is due to the fact that the zero-stress temperature (i.e. the temperature at which stress of restrained concrete is zero) is usually different over the cross-section of a member ("zero-stress temperature gradient"). Stresses of the member are zero only if the actual temperature gradient is the same as the zero-stress temperature gradient. For an arbitrary state of concrete temperatures the cracking risk may therefore be high or low as well, depending on the shape of the zero-stress temperature gradient. For the latter, the hardening temperatures during the first day of hydration (i.e. when the degree of hydration is still low) are decisive.

Cervera *et al.* (1999) from the International Center for Numerical Methods in Engineering (CIMNE) in Barcelona have developed a numerical model for coupled thermo-chemo-mechanical process, considering many of the relevant features of the hydration and aging of concrete, in a format

suitable for its implementation in the general framework of the Finite Element Method. This model is able to accurately predict the evolution in the hydration heat production and the main mechanical properties of concrete. Therefore a prediction of the evolution of thermally induced stresses in concrete at early ages can be made.

The prediction of the development of temperature and the mechanical properties during hydration by the model has been verified by simulation on dams and other massive concrete constructions. Until now the prediction of stresses by the model could not be verified precisely enough due to the difficulties of measuring the stresses in young concrete. In concrete dam construction for instance only thermal deformations are usually measured. Transformation from deformations into stresses at early ages is not possible due to strong visco–elastic behaviour of young concrete. The question how to determine the right reference temperature (used for the calculation of thermal strains in the model) has still to be solved.

Mangold (1994) simulated the stress development in different parts of an one meter thick wall. Continuous measurements of the stresses in different parts of the wall, subject to different temperature histories, could be done with the help of a so called "cracking frame". A numerical simulation of this experiments gives now the possibility to verify the stress prediction by the constitutive model. The comparison between the experiments and the prediction also help to discuss the influence of the viscous effects, the importance of the reference temperature and the chemical content of the concrete.

1.2 Overview

This work is subdivided in the following chapters:

Chapter 2 gives an introduction to the development of stresses during the hydration of concrete. On the basis of the doctoral thesis of Mangold (1994) the behaviour of the zero-stress temperature in concrete members of 30 cm or more will be described.

Chapter 3 outlines the thermo-chemo-mechanical model developed by Cervera *et al.*(1999).

Chapter 4 presents the numerical simulation and the sensitivity analysis of three experimental cases studied by Mangold (1994). This simu-

lation is carried out with the finite element program COMET (COupled MEchanical and Thermal Analysis) using the constitutive model developed by Cervera *et al.* (1999). Starting from a given development of temperature from Mangold (1994), the prediction of stress development in different parts of a wall is made. The model is assessed by comparing the experimental results with the prediction by the model. The main attention will be set on the influence of the reference temperature used for the calculation of thermal strains and the visco–elastic effects on the development of the stresses during the first days of hydration. The simulation of experiments with different concretes helps to discuss the chemical part of the model.

Chapter 5 contains some concluding remarks, summarizing the major results of this work. Moreover, suggestions for future research direction, regarding a possible modification of the constitutive model, are presented.

Chapter 2

Behaviour of Young Concrete

2.1 Development of Temperature

Hydration of cement is a very complex and highly exothermal process. The development of the temperature in young concrete depends on a high ammount of parameters, such as hydration heat and the hydration degree, the thermal properties and on the setting conditions. In the following section the state of art given in Mangold (1994) is summarized.

Hydration heat

The hydration heat $Q(t)$, produced due to the hydration of concrete, depends on the chemical composition and/or on the fineness of the cement. Basically, the free water present in the mixture reacts with the unhydrated cement to form hydrates. Portland cement is formed by four main mineral constituents: calcium silicates like C_3S and C_2S, calcium aluminates like C_3A and calcium aluminoferrites like C_4AF. They react and combine with water to form differents hydrates: calcium silicate hydrate CSH, calcium hydroxide CH, ettringite Aft, monosulfate Afm, etc. The hydration mechanisms have been investigated for the last hundred years, but they are not clearly understood. However, it is clear that the rates of reaction of the individual constituents differ quite significantly. The hydration heat released in the first day after pouring depends mostly on the existence of C_3S and C_3A, see Lochner (1984). Breitenbücher (1994) proved for low-alkali cements that a low alkali content (K_2O, Na_2O) and high sulphate content

related to C_3A lead to a low temperature development.

The rate of hydration of the cement highly depends on the temperature while pouring and the development of temperature during hydration. The higher the temperature of concrete the faster the development of hydration. For this reason hydration accelerates itself in thick members, where the release of hydration heat is very small.

To get information about the state of hydration at any time and temperature conditions, the hydration degree $\xi(t)$ is defined. It can be expressed as the ratio of the actual heat release $Q(t)$ to its maximum in ideal conditions $\bar{Q}_\infty$,

$$\xi(t) = \frac{Q(t)}{\bar{Q}_\infty} \tag{2.1}$$

The final value of the hydration degree in ideal conditions is $\xi = 1\,(100\%)$. In practice, these conditions are not fulfilled during curing and complete hydration of the concrete is not achieved. The final degree of hydration ξ_∞ is related to the water/cement ratio of the mixture and it can be estimated as a function of it as, see Mills (1996).

$$\xi_\infty = \frac{1.031\, w/c}{0.194 + w/c} \tag{2.2}$$

Thermal Properties

The thermal properties of concrete such as the thermal conductivity k_T and the heat capacity C do also change with the temperature, the moisture content and the hydration degree of the concrete. Anyhow investigations by Hamfler (1998) show that calculation with constant values give sufficiently accurate results.

Setting Conditions

Hydration also depends on the setting conditions like:

- proportion of the surface and the volume of the member;
- temperature difference between the concrete and the environment;
- air humidity and loss of moisture in the concrete;

- heat transmission between the surface of the concrete member and the environment depending on solar radiation α_s and on convection α_k such as windvelocity and temperature difference between the concrete and the environment;
- thermal resistence of the formwork;
- time of formwork stripping and the ambient conditions at that time;
- after treatment.

2.2 Basis of Stress Development

The stress development in young and unloaded concrete is due to hindered thermal and nonthermal deformation. The following section explains these phenomena.

Thermal Deformation

Thermal strain ε_T is caused by the heat of hydration or external temperature effect and the resulting change ΔT in temperature of the concrete element. Its magnitude is determined by the coefficient of thermal expansion α_T [1/K] of the concrete:

$$\varepsilon_T = \alpha_T \Delta T \tag{2.3}$$

The thermal expansion coefficient of the concrete α_T depends on the expansion coefficient of the aggregates and also on the development of hydration. α_T of hardened concrete is 8 to 10 times smaller than the coefficient of the fresh concrete. However, investigations by Boulay (1994) showed that for calculations of thermal stresses a constant value can be admitted.

Nonthermal Deformation

Nonthermal strain $\varepsilon_{s,sw}$ is caused by shrinkage and swelling of the concrete. It can be distiguished between three types of shrinkage at early age, see Schöppel (1994):

1) Plastic and early shrinkage which occur as a result of capillary force in the plastic non hardened concrete due to loss of water.

2) Chemical shrinkage which occurs because the volume of the reaction products is less than the sum of the volumes of the original constituents, i.e. the water and the anhydrous cement. If water cannot penetrate from outside into the concrete, internal self-desiccation occurs and causes a contraction of the concrete volume.

3) Drying shrinkage of the hardening concrete by loss of moisture.

Type 1 and 3 of shrinkage only occur if the concrete is not protected sufficiently against moisture loss, for the latter the moisture change during hydration in thicker concrete members is negligible, Mangold (1994).

Swelling of the concrete can be caused by the absorption of water and/or the chemical reaction of the sulphate components of the cement (chemical swelling), see Schöppel (1994).

The nonthermal deformations are defined in accordance with their cause and their time of occurrence as: primary chemical shrinkage (I) and chemical swelling (II), secondary chemical shrinkage (III), secondary swelling (IV) and tertiary shrinkage (V).

Degree of Restraint

The development of stresses is due to hindered internal deformation in the concrete member. One can distinguish between intrinsic and restraint stresses, see Figure 2.1.

Intrinsic stresses are due to the Bernoulli hypothesis that the cross-sections remain plane. Neighbour layers want to deform differently. These stresses are self equilibrating (see Figure 2.1) and do not result in external forces.

Restraint stresses are due the bearing. The degree of restraint δ gives information about the boundary conditions of the member and is defined as the proportion of restraint deformation to the deformation which would occur under free possibility of displacement. Its magnitude is very difficult to establish. During the first hours of hydration, while the Young modulus is still low, the degree of restraint is 100 %. With the increasing of the Young modulus the degree decreases in magnitude between 50%-80%.

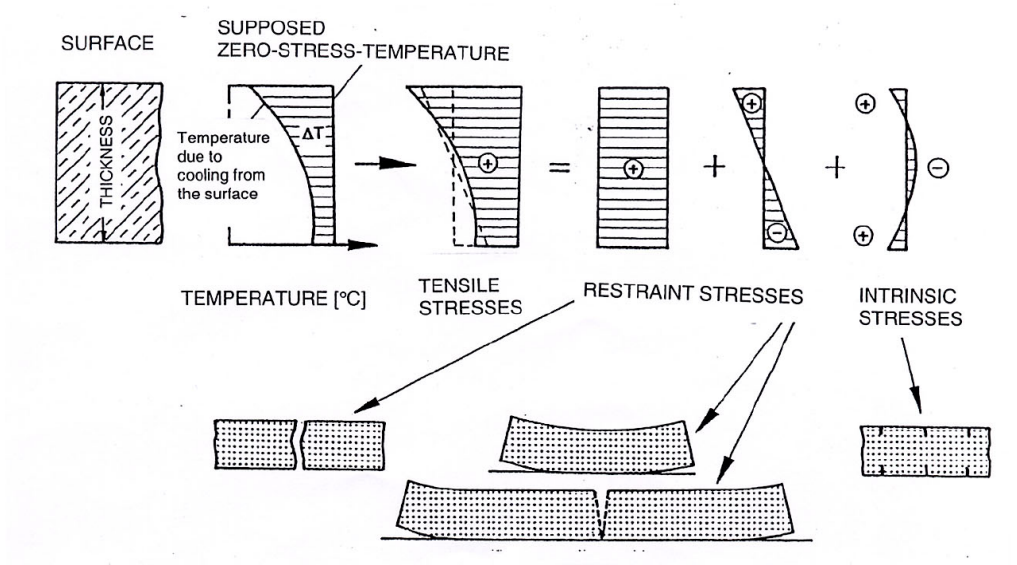

Figure 2.1: Partitioning of the Stresses due to Surface Cooling and full Restraint in a Concrete Slab. A constant Zero-Stress Temperature is assumed.

Mechanical Properties

The magnitude in which the hindered deformation in young concrete is transformed into stresses depends on the development of the mechanical properties (e.g. Young modulus and relaxation).

Creep is the time dependent increase of deformation under constant stresses. Relaxation is the time dependent decrease of stresses under constant deformation. This phenomenon is due to the viscoelastic behaviour of the concrete.

The greatest part of the deformation due to the creep and relaxation is caused by the hardening process of the cement. The bigger the volume of the hardened cement and the higher the water/cement ratio, the more significant is creep. The cement's velocity of hardening is influencing. The slower the hardening of the cement, the higher the creep deformation. The higher the temperature, the bigger the deformation due to creep.

Rheological Model

Summarizing, the total strain in a concrete member is the result of the strain due to microcracks, the elastic deformation, creep and the load-independent

deformation such as thermal deformation, chemical shrinkage or chemical swelling, deformation due to moisture loss. One of the first rheological models that takes all these effects into account was developed by Bažant and Chern(1985), see Figure 2.2.

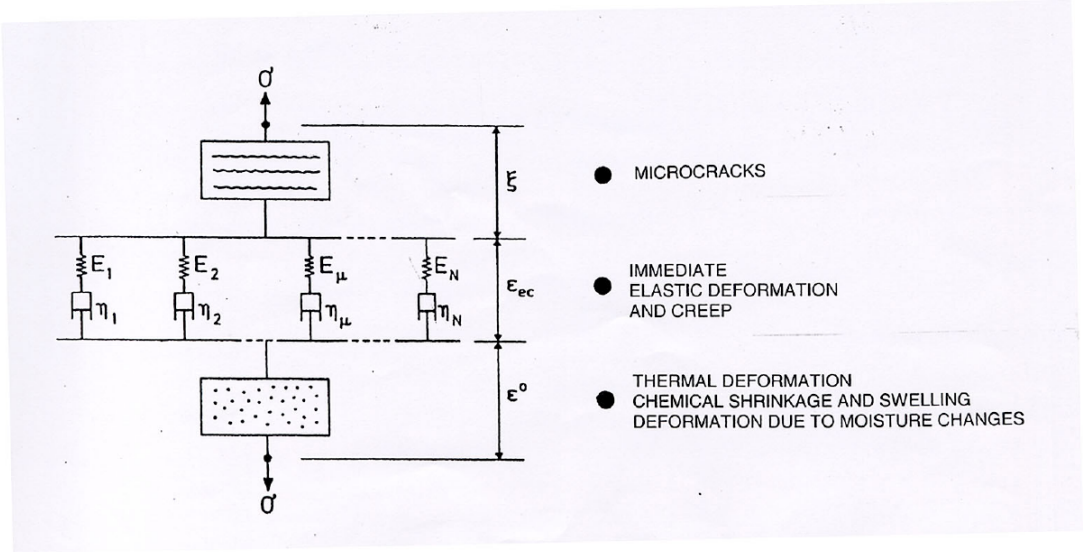

Figure 2.2: Rheological Model representing the total Strain in Concrete, Bažant and Chern (1985).

2.3 Development of Stresses

The development of stresses depends on all the parameters mentioned above, as it will be described in the following section. Also, the concept of the zero-stress temperature is introduced (temperature at which the stress of the restrained concrete is zero).

Development of Stresses and the Zero-Stress Temperature

Concrete members with a thickness of 30 cm or more heat up considerably due to the heat of hydration of the cement. If concrete would be a

linear-elastic material with a constant Young modulus (i.e. like steel under normal temperature and loading conditions, under the yield strength) the hydration heat was transformed into compressive stresses under restrained deformation. The compressive stresses would become zero once the initial temperature was reached again. For the latter, there would always be stress-free conditions if the initial temperature was equal to the temperature in the concrete, see Mangold (1994).

But young concrete is not a linear-elastic material: during the heating phase the concrete's Young modulus increases and relaxation is high. If concrete hardens under restraint, the hindered expansion (during which the temperature increases) is largely transformed into viscous strain of the concrete.

In the first three to six hours the concrete remains in stress-free conditions even if the temperature raises, see Figure 2.3. This is the unfavorable part of hydration heat: the heating does not produce compressive stresses but the later cooling produces considerable tensile stresses.

The development of concrete temperature $T(t)$, the corresponding restraint stresses $\sigma(t)$ and the zero-stress temperature $T_z(t)$ of a concrete member under complete restraint is shown in Figure 2.3, see Mangold (1994).

Note that during the first hours the actual zero-stress temperature is the same as the actual concrete temperature. $T_{z,1}$ is defined as the transition from purely viscous to viscoelastic behaviour of the concrete. Hence one portion of hindered deformation results in stress ("elastic deformation"), the other part results in inelastic deformation of the concrete (relaxation, microcracks) and not in stress. However, modulus of elasticity of concrete is still low and the relaxation is high, so that the development of stresses is quite slow.

The more the degree of hydration and thus the stiffness of the concrete increases, the hindered expansion is transformed into stresses and the portion of the inelastic deformation becomes smaller. Therefore, the course of the zero-stress temperature T_z deviates more and more from the course of the concrete temperature and approaches an almost constant value. When the temperature maximum is exceeded and the concrete cools down, considerable tensile stresses are produced so that the compressive stress rapidly decreases, see Figure 2.3. The concrete is stress-relieved at the zero-stress temperature $T_{z,2}$.

Cracking frame tests, which will be described in more detail in Section 2.4, made it possible to quantify zero-stress temperatures from the onset of hydration. $T_{z,2}$ is considerably higher than the initial temperature and often only a few degrees lower than the maximum temperature. However, $T_{z,2}$ as shown in Figure 2.3 is only a single point within the whole range of the temperature development, at which the stress of the restrained concrete is actually zero. In fact corresponding to any arbitary state of stress $\sigma(t)$ there is also a value $T_z(t)$, the "actual zero-stress temperature", at which the actual stress would be zero under the given degree of restraint. If the actual concrete temperature $T(t)$ is higher than the actual zero-stress temperature $T_z(t)$ compressive stresses occur in the case of restraint. If $T(t)$ is lower than $T_z(t)$, tensile stresses occur.

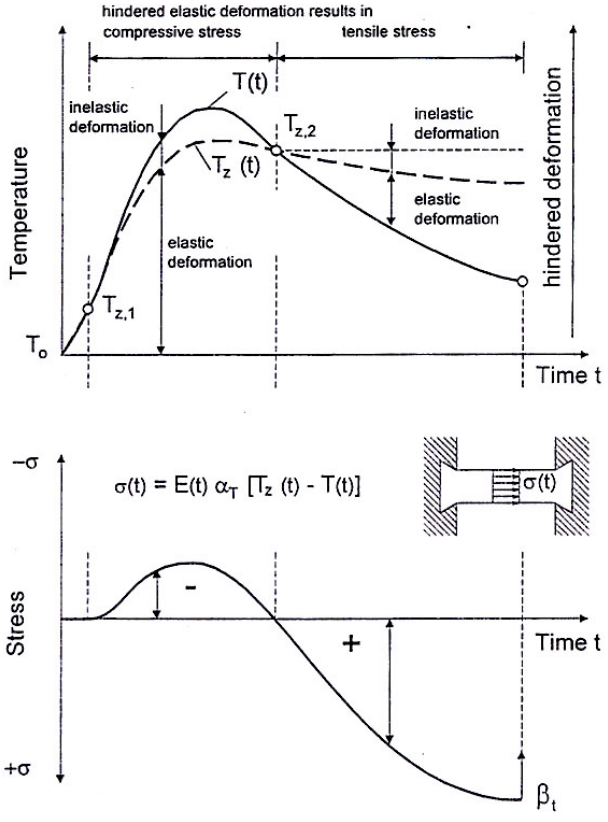

Figure 2.3: Development of concrete temperature $T(t)$, restraint stress $\sigma(t)$ and zero-stress temperature $T_z(t)$ if the concrete hardens under restraint.

Zero-stress Temperature Gradient

The phenomenon the zero-stress temperature T_z can be explained with Figure 2.4. It is commonly assumed that there is a constant zero-stress temperature over the cross-section of a concrete member, see Figure 2.4 a).

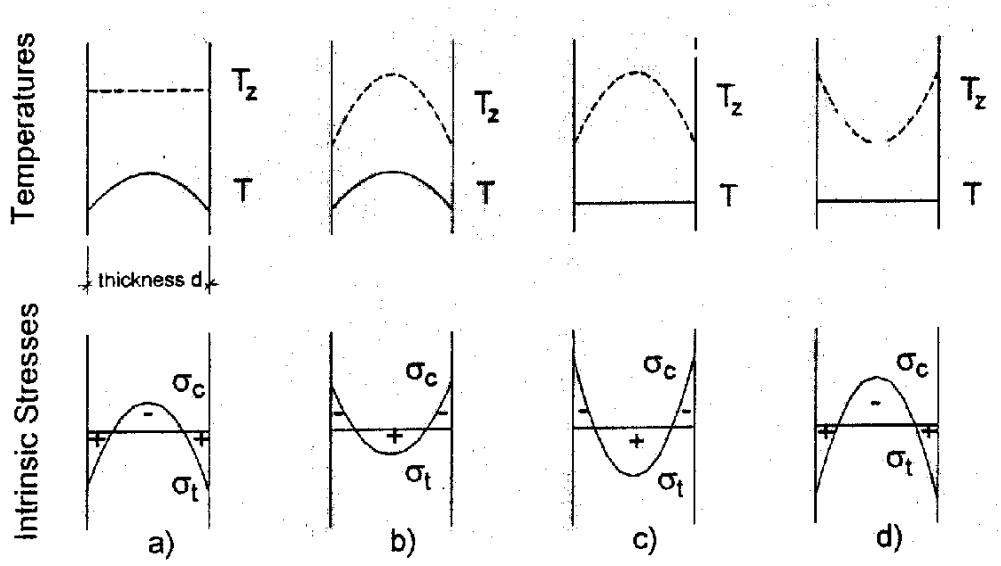

(a)

Figure 2.4: Stress Development and the zero-stress temperature in the wall

But experimental research by Mangold (1994) show that the temperature development due to the heat dissipation varies depending on the location in the cross-section. The effect of different zero-stress temperatures is obvious. Supposing different definition of the course of T_z the intrinsic streses varies significantly. If the gradient of T_z is more convex than the curvature of the temperature gradient, T, compressive stresses occur at the surface of the member, while in the centre tensile stresses occur, see Firgure 2.4 b). If the ambient temperature is reached again compressive stresses remain at the surface, see Figure 2.4 c). If the gradient of T_z is concave tensile stresses would occur st the surface of the member.

Considering the whole cross-section of a concrete wall, the member hardens with a curved zero-stress temperature gradient, see Figure 2.5. The temperature difference between the temperature gradient and the actual zero-stress temperature gradient leads to thermal stresses. Because the zero-stress temperatures at the surface and in the center of the member still develop during hydration (see Figure 2.3) also the zero-stress temper-

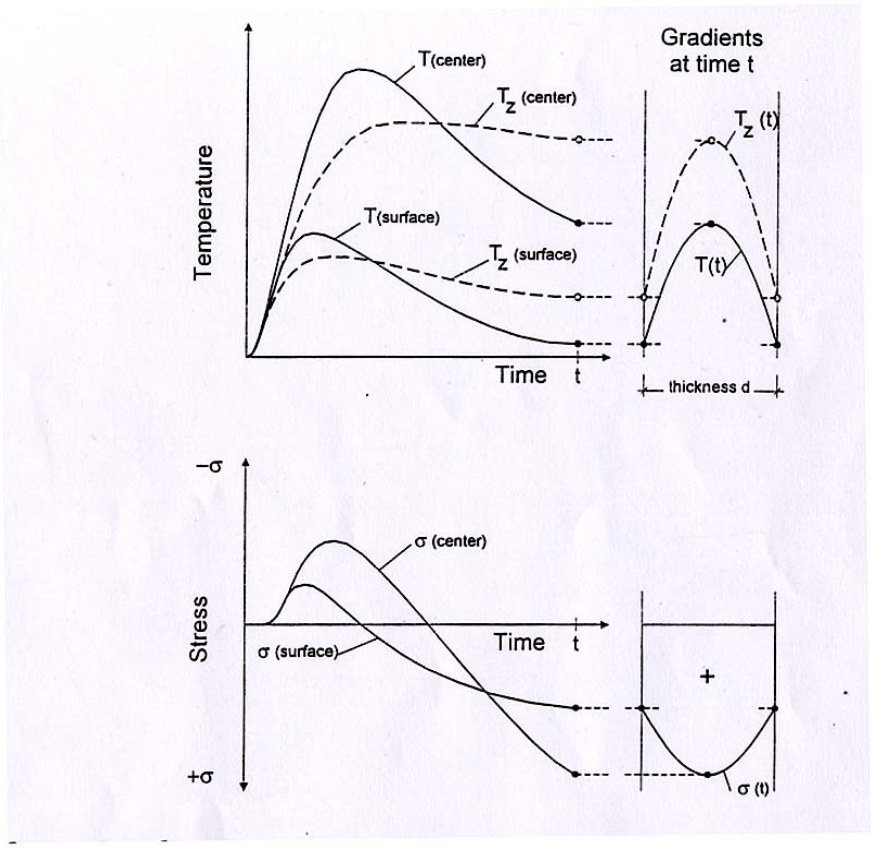

Figure 2.5: Development of concrete temperature (T), zero-stress temperature (T_z) and stress (σ) at the surface and the center of the wall.

ature gradient is not constant during the early stage of hydration ("actual zero-stress temperature gradient"). Concrete temperatures during the first day of hardening are therefore decisive for the magnitude of the zero-stress temperature. If the concrete hardens at high zero-stress temperatures (e.g. on hot summer days) the thermal tensile stresses and thus also the risk of cracking of the member will be high. If the zero-stress temperatures are low, so will be the thermal tensile stresses and thus the risk of cracking is low. Judging thermal stresses and the risk of cracking from temperature measurements one has to take the zero-stress temperature gradient into account.

2.4 Experimental Investigations by Mangold (1994)

The objective of this diploma thesis is to verify the stress prediction by the constitutive model developed by Cervera *et al.* (1999). The experimental investigations by Mangold (1994) represent the most relevant phenomena which influence the development of temperature and thus the development of stresses in young concrete. Therefore they are ideal to use for the numerical simulation of the stress development and its analysis.

Mangold's Objective

As the previous sections show, the development of stresses in concrete members depends on a high ammount of parameters. Besides the heat of hydration is not only very important for massive concrete constructions but also for members about 30 cm in thickness and more. In such cases the maximum temperature is reached about one day after pouring. The concrete then requires about one week to cool down to the ambient temperature. For the calculation of restraint and intrinsic stresses in young concrete commonly a constant zero-stress temperature was admitted. As it is explained in the previous sections, this is not reliable. Therefore the objective of Mangold's Doctoral Thesis was to find a method to determine the development of the zero-stress temperature and its gradient in an arbitrary portion of the cross-sections of concrete members more exactly than up to date. Hence a more accurate quantification of restraint and intrinsic stresses in young concrete and a risk of cracking prediction was possible. Mangold chose to analyse the development of stresses in a wall of one meter thickness.

Mangold's Work

The continuous change in the concrete properties results in a nonsimultaneous development of temperature and thermal stresses. Due to these difficulties, measurements of stresses directly in the wall are not possible. Comparitive tests in the laboratory are necessary to study the restraint stresses and thermal cracking in concrete at early ages. For this purpose a special test device, the so called "cracking frame" which is shown in Figure 2.6, was developed at the Institute of Building Materials at the Technical

University of Munich.

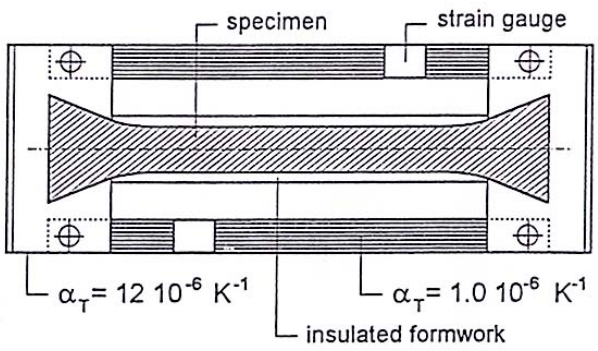

Figure 2.6: The Cracking Frame

The ends of the 1 meter long beam specimen (the concrete) are held by dovetails in two steel cross-heads. In order to keep the distance between the two cross-heads as constant as possible, they are connected with two steel longitudinal bars. A special steel with an extremely low thermal expansion coefficient $\alpha_T = 1.0\,10^6\,1/K$ is used. The concrete cross-section has to be chosen quite small for practical reasons, 15 x 15 cm^2. The formwork has a thermal insulation in order to reproduce the temperature development in a cross-section. The continous measurings of deformations by the strain gauge allow to quantify longitudinal stresses and thus the zero-stress temperatures.

Mangold (1994) wanted to study the development of stresses, thus the development of the zero-stress temperature and its gradient in one meter thick walls. To simulate the hardening process in different parts of the wall each beam specimen was heated according to the temperature development in one portion of the cross-section of the wall. This temperature development was calculated in advance with a finite-element program, see Mangold (1994). A constant ambient temperature of $T_a = 20\,°C$ and a wind velocity of $v = 2\,m/s$ was assumed for the temperature calculations. The temperature of the fresh concrete was assumed to be 20 °C. The wall was protected from the influence of solar radiation.

As one can see in Figure 2.5 the course of the gradient of T and T_z differ significantly next to the surface of the wall. Therefore Mangold studied the development of stresses in three different locations of the cross-section of the wall: at the centre ($x = 0.5\,m$), at the eighth ($x = 0.12\,m$) and at the surface ($x = 0.0\,m$), see Figure 2.7.

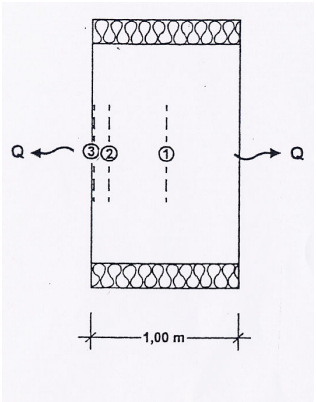

Figure 2.7: Mangold studied the Development of Stresses in the three locations of the Cross-Section of a Wall with one meter thickness: at the Centre (1), the Eighth (2) and the Surface (3).

The Experiments

In order to study the development of stresses and thus the effect of zero-stress temperature, Mangold proposes a variety of experiments. Among other experiments, Mangold investigated the heat production in walls with different concretes and different formworks.

Influence of Cement's Content: Hydration highly depend on the cement's content. Breitenbücher (1994) proved for low-alkali cements that a low alkali content (K_2O, Na_2O) and high sulphate content related to C_3A lead to a low temperature development and thus a low cracking temperature. Besides the development of the Young-modulus and the tensile strength is slower. Therefore Mangold tested two different types of cements from different plants, the concrete MKA and MKL. A significant result of the other type of cement is the cracking tendency, such as:

- **Concrete MKA:** with a high cracking tendency.
- **Concrete MKL:** with a low cracking tendency.

The experimental investigations show that the development of stresses of both concretes are very different, see Figure 2.8. The development of hydration heat of MKA is faster and higher. The higher the heating, the higher the zero-stress temperature. The development of nonthermal deformation such as chemical shrinkage and swelling also dues to the cement content and is very important for the development of stresses. Significant chemical swelling over a long period results in restrained concrete in compressive

stresses. Thus tensile stresses during cooling get smaller. At the same time the second zero-stress temperature is getting smaller, which means that the evolution of tensile stresses begins later, with smaller temperatures. For the latter tensile stresses and thus the risk of cracking is higher by hindered chemical swelling. Figure 2.8 also represents this phenomena. After four days both concretes reach the initial temperature. Then the members were cooled down artificially until the concrete cracked. Note that at the end of hydration the concrete MKL achieved only 50% of its tensile strenght, while concrete MKA allready consumed 80% of it. As the cement of MKL has a lower alkali content (K_2O, Na_2O) than MKA, the results of investigations by Breitenbücher (1994) are proved once again.

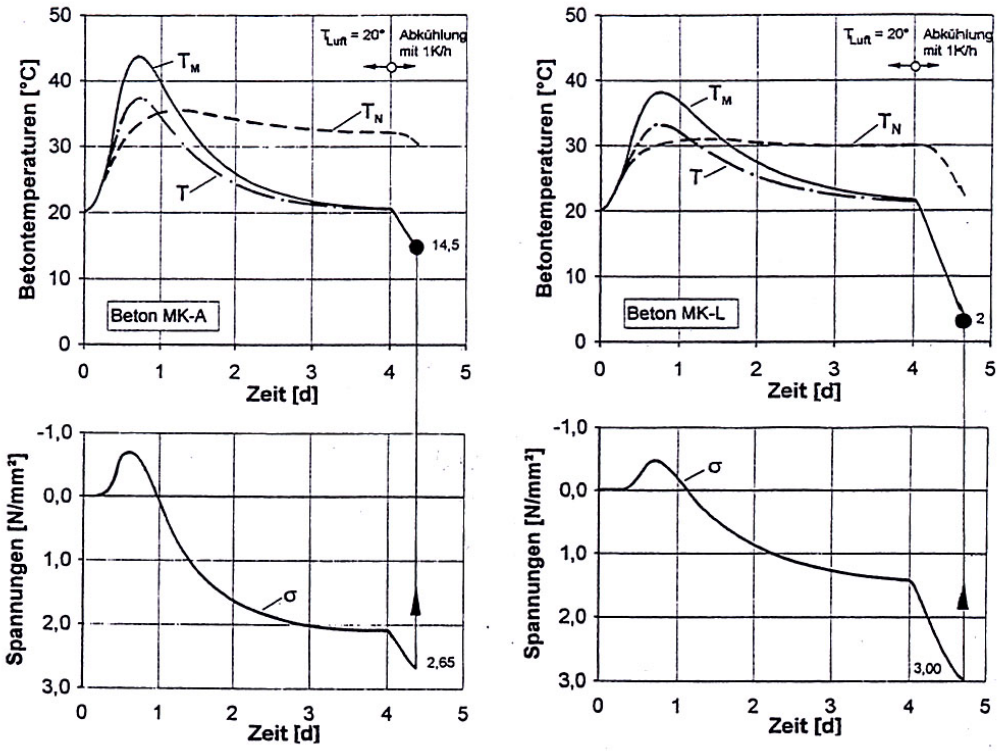

Figure 2.8: Development of concrete temperature and stresses in two different concretes: MKA (high cracking tendency) and MKL (low cracking tendency). After four days both concretes reach the initial temperature, the tensiles stresses differ significantly. Then the members were cooled down artificially until the concrete cracked (Mangold (1994)).

Influence of different formwork: It is obvious that the development of temperature in a concrete wall depend highly on the heat transfer with the environment. Therefore Mangold studied the hardening process of walls with different types of formwork. Mangold did these experiments with both type of concretes.

- **Steel Formwork:** The heat transfer at the surface of a one meter thick wall was almost unhindered as in the case of a steel formwork. The formwork was stripped after 48 hours. Both concretes, MKA and MKL were studied.
- **Wooden Formwork:** The heat transfer at the the surface of the wall was inhibited by a heat insulating formwork. The formwork was stripped after 48 hours. Once again both concretes, MKA and MKL were studied.

Chapter 3

Thermo-Chemo-Mechanical Model by Cervera *et al.* (1999)

This work is focused on the numerical simulation of development of thermally induced stresses during hydration of young concrete. The program COMET has many calculation possibilities. In the following chapter a short overview over the program and the constitutive model, developed by Cervera *et al.* (1999), is given.

3.1 Thermo-Mechanical Problem

3.1.1 Thermo-mechanical Interactions

The hardening process of concrete is divided into different subproblems depending on each other, such as:

- chemical problem,
- thermal problem and
- mechanical problem.

The chemical problem (problem of hydration and aging) is represented by only one variable such as the hydration degree of the concrete which describes the development of the microstructure of the material. It shows the complex phenomenon of the hydration and hardening of the cement and controls the quantity and velocity of the hydration heat and the development of the material mechanical properties.

The thermal problem consists on the evaluation of the thermal history of the concrete. This evaluation can be done by using the equation of energy, which is produced for the volume of the material. The fundamental variable of this problem is the temperature. The method used to study this problem is framed into the phenomenological theory, which means in this context that it is based on a macroscopic approach.

Finally, for the mechanical problem the conditions of equilibrium must be satisfied by the stresses developed during the studied process. The method to study this problem is also framed into the phenomenological theory.

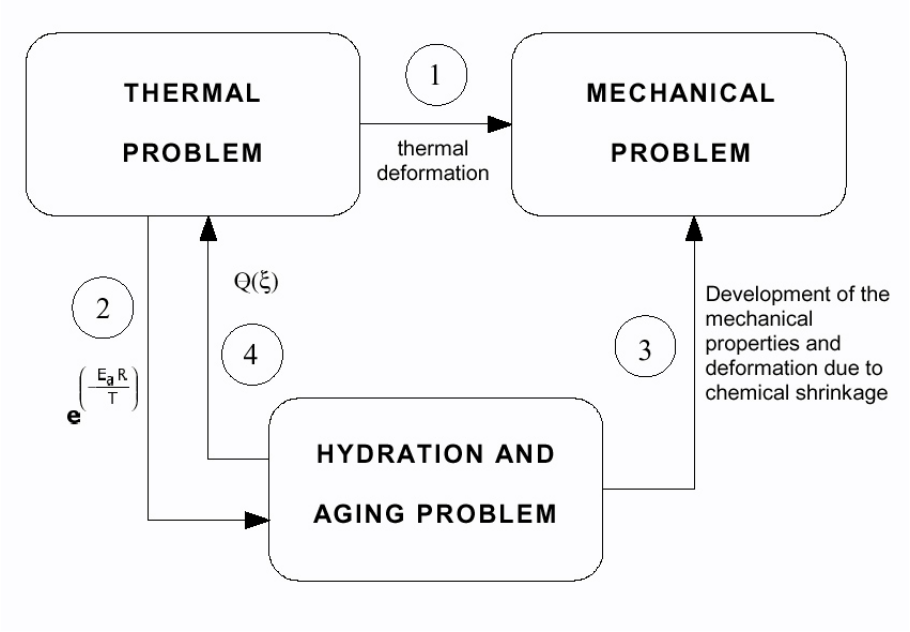

Figure 3.1: Thermomechanical Interactions for Concrete at Early Ages.

The coupling between these three problems can be sufficiently described with four interaction. They are visualized with the help of the scheme given in Figure 3.1.

Interaction 1 (thermal problem $\longrightarrow$ mechanical problem) refers to the thermal deformations and consequently to the thermally induced stresses within the constitutive model which depend on the temperature.

Interaction 2 (thermal problem $\longrightarrow$ chemical problem) conditons the microstructural transformation of the concrete. Therefore all the micro-

scopic phenomena which are involved in the process of hydration and aging, together with other variables are related to the temperature at which they develop.

Interaction 3 (chemical problem $\longrightarrow$ mechanical problem) refers to the development of the thermal and mechanical properties of the concrete during the process of hydration. It also generates volumetrical deformations of the concrete due to hydration (chemical shrinkage).

Interaction 4 (chemical problem $\longrightarrow$ thermal problem) governs the energy changes derived from the phenomenon of hydration of the cement. This heat release modifies the local thermal history of the concrete.

3.1.2 The Governing Equations

The local system of partial differential equations governing the coupled thermo-mechanical problem is defined by the momentum and energy balance equations. They can be written as:

$$\begin{cases} C\,\dot{T} - \dot{Q}\,(\xi) = R_{ext} - \nabla \cdot \boldsymbol{Q} \\ \\ \mathbf{0} \quad = \nabla \cdot \boldsymbol{\sigma} + \boldsymbol{b} \end{cases} \tag{3.1}$$

where C is the heat capacity, T the temperature, R_{ext} represents the heat production of the external volume heat sources and $\boldsymbol{Q}$ is the heat flux. In the momentum equation $\boldsymbol{b}$ describes the body forces, $\nabla \cdot (\cdot)$ is the divergence operator and $\boldsymbol{\sigma}$ is the stress tensor.

3.1.3 Time Integration of the Coupled Model

The numerical simulation of the coupled thermo-mechanical problem involves the transformation of a system of differential governing equations into a sequence of discrete algebraic problems by means of a Galerkin finite element projection and a defined time marching scheme.

Time marching schemes for the advancement of the main variables (displacements and temperatures) can be grouped in two categories: simultaneous time-steppimg algorithms and staggered time-stepping algorithms.

Simultaneous time-stepping algorithms solve both, the mechanical and the thermal equilibrium equations together, thus advancing of the displacements and temperatures, simultaneously. It leads to large and unsymmetric systems of equations and usually it is expensive to solve.

Staggered time-steppimg algorithms are based on the use of an operator split, applied to the coupled system of differential equations, and a product formula algorithm, which leads to a scheme in which each on of the subproblems defined by the partitions is solved sequentially, within the framework of the classical fractional step method. This leads to the partition of the original coupled problem into smaller and typically symmetric subproblems. In COMET this staggered scheme has been preferred.

In the classic isothermal split the coupled system of equations is partitioned into a mechanical phase at constant temperature, followed by a thermal phase at fixed configuration. In both phases the internal variables Γ_n, such as the damage tensile/compressive thresholds (r^+,r^-), respecting the micro prestress (μ), hydration degree (ξ) and aging degree (κ) are updated.

The stress development during the early ages of concrete is basicly activated by the variation of temperature. Therefore it is advantageous to consider a sheme where the thermal phase of the operator split is performed before the mechanical phase. The mechanical problem is then solved by using the updated field temperature, T_{n+1}. Table 3.1 represents the two phases at each time step. The time integration of a quasi-static problem consists of finding the amounts of the displacements u_{n+1} and the temperatures T_{n+1} from a known solution of u_n and T_n. In COMET a Backward Euler scheme is used.

Thermal Problem
u_n, T_n and Γ_n
$\downarrow$
u_n, T_{n+1} and $\tilde{\Gamma}_{n+1}$
Mechanical Problem
u_n, T_{n+1} and $\tilde{\Gamma}_{n+1}$
$\downarrow$
u_{n+1} and Γ_{n+1}
u_{n+1}, T_{n+1} and Γ_{n+1}

Table 3.1: Scheme for Advancing in Time

3.2 The Constitutive Model

The following section presents the thermo-chemo-mechanical model developed by Cervera *et al.* (1999) which considers many of the relevant features of the hydration, aging and mechanical behaviour of concrete, in a format suitable for its implementation in the general framework of the Finite Element Method.

3.2.1 Hydration and Aging Model

Hydration Model

From the first and second principles of thermodynamics the thermal field equation can be written, as

$$C\,\dot{T} - \dot{Q}(\xi) = R_{ext} + k_T\,\nabla\cdot(\nabla T) \tag{3.2}$$

where T is the temperature, C the heat capacity per unit volume, $\dot{Q}$ the velocity of liberated heat per unit volume, R_{ext} is the heat production of the external volume heat sources and k_T is the thermal conductivity. Note that the term due to the hydration heat, $\dot{Q}$, actually acts as a nonlinear internal heat source. Besides the Fourier's Law ($\boldsymbol{Q} = -\,k_T\,\nabla T$) has been use (see Eq. 3.1).

The thermo-chemical model must provide the determination of this term depending on the hydration heat. The thermo-chemical model regards the evolution of the chemical reaction of concrete hydration and the heat generated during the process. It is based on the Theory of Reactive Porous Media, within a consistent thermodynamic framework. The assumption of a closed chemical system allows a local description of the internal variables.

For practical purposes, it is convenient to write the model in terms of a normalized variable called hydration degree, ξ. Most authors identify the rate of liberated heat with the rate of the hydration. In this case, the hydration degree can be also defined $\xi = Q/\bar{Q}_\infty = \xi_\infty < 1$, where $\bar{Q}_\infty$ is the final amount of liberated heat in ideal conditions. (The final degree of hydration ξ_∞ can be estimated with the Eq. 2.2.) This is equivalent to assume a linear dependency of the form

$$Q(\xi) = Q_\xi \xi \tag{3.3}$$

where Q_ξ is the latent heat, here assumed a constant material property.

By assumming that the hydration reaction is thermoactivated, development of hydration degree can be defined with an Arrhenius type equation such as

$$\dot{\xi} = \tilde{A}_\xi(\xi) \exp\left(-\frac{E_a}{RT}\right) \geq 0 \tag{3.4}$$

where E_a is the activation energy of the reaction, R is the constant for ideal gases, see Ulm and Coussy (1996). The ratio E_a/R can be experimentally determined, and it ranges from 3000 to 8000 K for concrete. The function $\tilde{A}_\xi(\xi)$ represents the normalized affinity that completely characterizes the macroscopic hydration kinetics for a given concrete mixture. This function can also be obtained experimentally from an adiabatic calorimetric test. In this model the following expression with the material constants, such as k_ξ, $A_{\xi 0}$, $\eta_{\xi 0}$ and $\overline{\eta}$, is proposed:

$$\tilde{A}_\xi(\xi) = \frac{k_\xi}{\eta_{\xi 0}} \left(\frac{A_{\xi 0}}{k_\xi \xi_\infty} + \xi\right) (\xi_\infty - \xi) \exp\left(-\overline{\eta}\frac{\xi}{\xi_\infty}\right) \tag{3.5}$$

Aging Model

The change in the relative proportions and physical properties of the basic constituents of concrete during the chemical reaction of hydration is a phenomenon known as aging.

During the last decades, many aging models have been proposed in which the mechanical properties of young concrete were expressed in terms of the hydration degree, or alternatively, of the maturity. The basic assumption for these models is that concretes of the same mix at the same hydration degree have the same strength independently of the hydration kinetics occurred to reach that hydration degree.

However, there is experimental evidence (see Chapter 2) that the evolution of the concrete strength depends not only on the degree of hydration, but also on the kinetics of the hydration reaction. In view of this, it is concluded that concrete strength cannot be related directly to the hydration degree, and therefore, the mechanical properties cannot be obtained without the consideration of the hydration kinetics.

A realistic aging model must be established in which the mechanical properties act as internal-like variables, and their evolution laws must be formulated in terms of, at least, hydration degree and temperature.

The aging model regards the evolution of the compressive and tensile uniaxial strengths and the uniaxial elastic modulus during the hydration process of the concrete, These are the basic parameters used in the mechanical damage model. For simplicity, Poisson's ratio is assumed to remain constant. The effect of the curing temperature on the evolution of the compressive strength makes it necessary to relate this evolution to the hydration kinetics. Therefore an aging internal variable, κ, is introduced, so that the compressive strength, f^- can be written as

$$f^-(\kappa) = \kappa\, f_\infty^- \qquad\qquad \kappa \geq 0 \tag{3.6}$$

where f_∞^- is the final compressive strength. Note that κ can be considered a normalized strength variable. Thus, it will be called here *aging degree*.

The evolution of the aging degree must be related to the hydration kinetics and the temperature. The following equation clearly expresses the dependency of the aging variable both on the hydration degree and on temperature:

$$\dot{\kappa} \;=\; (A_f\,\xi \;+\; B_f)\,\Big(\frac{T_T - T}{T_T - T_{ref}}\Big)^{n_T}\,\dot{\xi} \tag{3.7}$$

where T_{ref} is the reference temperature for the determination of f_∞^-, T_T represents the maximum temperature at which hardening of concrete may occur and n_T is a material property.

The final tensile strength and the final elastic modulus are usually considered to be related to the final compressive strength and therefore to the aging degree, such as

$$f^+(\kappa) \;=\; \kappa^{2/3}\, f_\infty^+ \tag{3.8}$$

and

$$E(\kappa) \;=\; \kappa^{1/2}\, E_\infty \tag{3.9}$$

where f_∞^+ and E_∞ are the final values at the end of hydration.

3.2.2 Damage and Creep

The mechanical behaviour of concrete is complex and highly nonlinear. In order to describe the mechanical aspects of concrete the short and long term mechanical behaviour is modelled via a viscoelastic damage model which accounts for the aging effects.

The basic idea is to use a viscoelastic aging model, able to reproduce the creep and relaxation phenomena typical of long term behaviour of concrete. This must be coupled to a damage model, also considering the relevant thermal and chemical effects. Long term effects are included by incorporating a creep model inspired in the Microprestress-Solidification Theory.

The short term model is based on the framework of the Continuum Damage Mechanics Theory. It makes use of an isotropic damage model, with only two scalar internal variables to monitor the local damage under tension and compression, respectively. It takes the temperature effects and the phenomenon of aging into account.

Microprestress-Solidification Theory

The rheological model which is used to represent the long term mechanical behaviour of concrete consists of a viscoelastic chain, with the elastic moduli, E^i, and the dashpot viscosities, η^i, of the $i = 1, ..., N$ Maxwell elements as material parameters. It is also helpful to consider the elastic moduli, E^i, and the relaxation times of the dashpots, defined as $\tau^i = \eta^i / E^i$, as an alternative characterization of the chain.

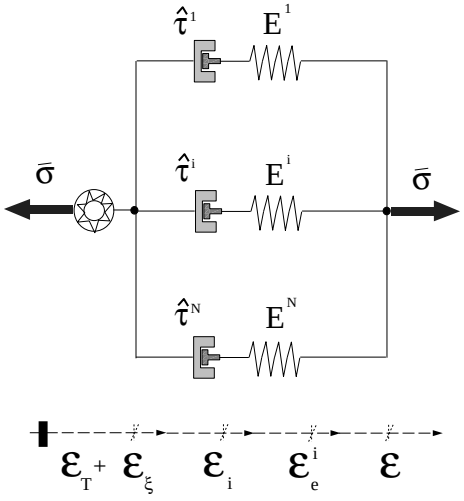

Figure 3.2: Rheological model for long term behaviour.

Figure 3.2 shows a schematic representation of the rheological model used for long term behaviour, in the form of a Maxwell chain. In the framework of aging models the general case of such a rheological model

would consist of independently varying elastic moduli and dashpot viscosities. However, it is usual to restrict the model to the consideration of proportional varying elastic moduli and constant relaxation times.

In the following it will be assumed that during the aging process all the elastic moduli vary proportionally to the aging function defined by the aging model, $E^i(\kappa) = \lambda_E(\kappa)\, E^i_\infty$ (where E^i_∞ are values at the end of the hydration process, and $E_\infty = \sum_{i=1}^N E^i_\infty$), and that the relaxation times, τ^i, remain constant. It was shown in Carol and Bazant (1993) that this is equivalent to the model arising from Solidification Theory, Bažant and Prasannan (1989), with a non-aging Maxwell chain for the basic constituent.

The total stress sustained by the Maxwell chain is evaluated as

$$\boldsymbol{\sigma} = \sum_{i=1}^{N} \boldsymbol{\sigma}^i \tag{3.10}$$

Choosing the stress in each Maxwell element of the chain, $\boldsymbol{\sigma}^i$, as internal variables, it was shown in Carol and Bazant (1993) that the first order differential equations governing the evolution of these variables are

$$\dot{\boldsymbol{\sigma}}^i + \frac{\boldsymbol{\sigma}^i}{\tau^i} = \lambda_E(\kappa) E^i_\infty \overline{\boldsymbol{D}}\, \dot{\boldsymbol{\varepsilon}} \quad \text{for} \quad i = 1, ..., N \tag{3.11}$$

where tensor entities are used as the multidimensional counterparts of the scalar ones used for uniaxial models; $\boldsymbol{\varepsilon}$ is the total strain tensor and the non-dimensional tensor $\overline{\boldsymbol{D}} = (1/E)\boldsymbol{D}$ has been used. where $\boldsymbol{D}$ is the (fourth order) linear–elastic constitutive tensor, which gives the information about the elastic behaviour of the material.

The proposed model cannot be the final solution of the long term aging because the duration of creep for a fixed load decreases significantly with an increasing age at loading even after many years, while the hydration degree essentially stops before one year of age. This experimental evidence was considered in the Solidification Theory, Bažant and Prasannan (1989), by including a flow element with a time dependent viscosity. A physical model is formulated to obtain the viscosity of the flow dashpot as a function of the tensile micro-prestress carried by the bonds and bridges crossing the gel pores in the hardened cement gel. The long term creep is assumed to originate from viscous shear slips between the opposite walls of micropores in which the bonds that transmit the micro-prestress break and reform. Let σ_μ be the value of the micro-prestress and η_μ be the value of the viscosity of the corresponding flow term.

With $\sigma_{\mu 0}$ and $\eta_{\mu 0}$ as initial values, it can be assumed that the viscosity is inversally proportional to the micro-prestress, so that $\sigma_\mu/\sigma_{\mu 0} = \eta_{\mu 0}/\eta_\mu = \mu$ where μ is a variable that can be regarded as the normalized value of the micro-prestress.

If humidity effects are not considered (sealed specimens, basic creep), the evolution of the normalized micro-prestress can be explicitly determined as: $\mu(t) = 1/(1 + c_{\mu 0}\, t)$, where $c_{\mu 0}$ is a material property. The relaxation time of the flow term as $\tau_\mu = (\tau_{\mu 0}\, E_\infty)/(\mu\, E)$ where $\tau_{\mu 0}$ is a material property. Note that as time increases, the micro-prestress decreases, and so the viscosity of the flow term increases. Eventually, the micro-prestress will vanish, the viscosity will tend to infinity and the flow term will become inactive.

Now, Eq. (3.11) has to be modified to include the effect of the nonlinear flow term:

$$\dot{\boldsymbol{\sigma}}^i + \Big(\frac{1}{\tau^i} + \frac{1}{\tau_\mu}\Big)\,\boldsymbol{\sigma}^i = E^i(\kappa)\,\overline{\boldsymbol{D}}\,\dot{\boldsymbol{\varepsilon}} \quad \text{for} \quad i = 1, ..., N \tag{3.12}$$

Instead of the stress, $\boldsymbol{\sigma^i}$, the viscous strains in each Maxwell element, $\boldsymbol{\varepsilon^i}$ can be selected as internal variables alternavily.

$$\boldsymbol{\sigma}^i = E^i(\kappa)\,\overline{\boldsymbol{D}} : (\boldsymbol{\varepsilon} - \boldsymbol{\varepsilon}^i) \tag{3.13}$$

Substitution of Eq. (3.13) into Eq. (3.12) leads to the obtention of the evolution law for the viscous strains

$$\dot{\boldsymbol{\varepsilon}}^i = \Big(\frac{1}{\tau^i} + \frac{1}{\tau_\mu} + \frac{1}{\tau_a}\Big)(\boldsymbol{\varepsilon} - \boldsymbol{\varepsilon}^i) = \frac{1}{\hat{\tau}^i}(\boldsymbol{\varepsilon} - \boldsymbol{\varepsilon}^i) \qquad \text{for} \quad i = 1, ..., N \tag{3.14}$$

with $\tau_a(\kappa) = E/\dot{E}$ representing the aging effect on the elastic modulus. Note that even if τ^i and τ_μ are sufficiently large, there would be some viscous straining as long as the aging progresses and the elastic modulus varies ($\dot{\lambda}_E \neq 0$). As time increases, the rate of hydration decreases, and so the viscosity due to aging increases. Eventually, $\tau_a(t = \infty) = \infty$ and the model would revert to a standard Maxwell viscoelastic arrangement.

Resuming the total relaxation time of the Maxwell chain depend on the summary of the inversial relaxation time of the dashpot, on the flow term, due to the micro-prestresses, and on the inversial relaxation time respecting the aging effect on the Young modulus, such as

$$\frac{1}{\hat{\tau}^i} = \Big(\frac{1}{\tau^i} + \frac{1}{\tau_\mu} + \frac{1}{\tau_a}\Big) \qquad \text{for} \quad i = 1, ..., N \tag{3.15}$$

Aging Viscoelasticity and Damage

The Continuum Damage Theory was firstly intoduced by Kachanov (1958) in the context of creep–related problems, but it has afterwards been accepted as a valid alternative to deal with complex material behaviour. It is nowadays used for a variety of materials as metals, ceramics, rock and concrete, and within a wide range of applications (creep, fatigue, progressive failure, etc.). The reason for its popularity is as much the intrinsic simplicity and versatility of the approach, as well as its consistency, based on the theory of thermodynamics of irreversible processes.

Finally the coupling of the viscoelastic model with a aging damage model is described, as well as the relevant thermal and chemical couplings. The basic hypothesis is that the stress sustained by the Maxwell chain is the effective (undamaged) stress, instead of the total stress. This idea is based on the Continuum Damage Mechanics Theory (CDMT) concept: the effective stress acts on the effective (undamaged) solid concrete, while the total stress acts on the whole (damaged) solid.

The effective stresses and the elastic strains for one element of the Maxwell chain can be defined as:

$$\overline{\boldsymbol{\sigma}}^i \left(\boldsymbol{\varepsilon}_e^i, \kappa\right) = E^i(\kappa)\, \overline{\boldsymbol{D}} : \boldsymbol{\varepsilon}_e^i \tag{3.16}$$

with

$$\boldsymbol{\varepsilon}_e^i(\boldsymbol{\varepsilon}, \boldsymbol{\varepsilon}^i, T, \xi) = \boldsymbol{\varepsilon} - \boldsymbol{\varepsilon}_T - \boldsymbol{\varepsilon}_\xi - \boldsymbol{\varepsilon}^i \tag{3.17}$$

where T is the temperature and ξ the hydration degree and (:) denotes the tensorial product contracted on two indices. Note that the thermal, $\boldsymbol{\varepsilon}_T = \alpha_T (T - T_{ref})\ \mathbf{1}$, and the chemical, $\boldsymbol{\varepsilon}_\xi = \alpha_\xi \xi\, \mathbf{1}$, volumetric strains affect all the elements in the same way, but the viscous strain tensor, $\boldsymbol{\varepsilon}^i$, is different for each Maxwell element.

The actual defined reference temperature T_{ref} in the constitutive model is equal to the temperature reached at the end of the setting phase (when $\xi = \xi_{set}$), so that the material begins the behaviour of a solide, and the process of thermally induced stresses starts. Values $\xi_{set} = 0.1$ to 0.4 have been proposed in the literature, depending on the type of cement and the water/cement ratio.

Inspirated by Faria *et al.* (1998) the stress split for each element, as

$$\overline{\boldsymbol{\sigma}}^{i+} = \sum_{j=1}^{3} < \overline{\sigma}_j^i > \boldsymbol{p}_j^i \otimes \boldsymbol{p}_j^i \qquad \text{and} \qquad \overline{\boldsymbol{\sigma}}^{i-} = \overline{\boldsymbol{\sigma}}^i - \overline{\boldsymbol{\sigma}}^{i+} \tag{3.18}$$

where $\overline{\sigma}^i_j$ denotes the *j–th* principal stress value from tensor $\overline{\boldsymbol{\sigma}}^i$, $\boldsymbol{p}^i_j$ represents the unit vector associated with its respective principal direction and the symbol $\otimes$ denotes the tensorial product. The symbols $< . >$ are the Macaulay brackets ($< x >= x,$ if $x \geq 0, < x >= 0,$ if $x < 0$).

The stresses are obtained with the following constitutive equation which relates the stresses with the deformation for each Maxwell element,

$$\begin{aligned} \boldsymbol{\sigma} &= (1-d^+)\sum_{i=1}^{N}\overline{\boldsymbol{\sigma}}^{i+} + (1-d^-)\sum_{i=1}^{N}\overline{\boldsymbol{\sigma}}^{i-} \\ &= (1-d^+)\,\overline{\boldsymbol{\sigma}}^{+} + (1-d^-)\,\overline{\boldsymbol{\sigma}}^{-} \end{aligned} \tag{3.19}$$

where two internal-like variables, d^+ and d^-, the damage indices under tension and compression, are introduced, respectively. The behaviour through time of d^+ and d^- are described by constitutive evolution equations.

Chapter 4

Numerical Simulation

The following chapter includes the numerical simulation of the stress development of the three case studies (see Section 2.4):

- **Case Study 1:** Wall with one meter thickness and steel formwork, the concrete with high cracking sensitivity is used (MKA).
- **Case Study 2:** Wall with one meter thickness and wooden formwork, the concrete with high cracking sensitivity is used (MKA).
- **Case Study 3:** Wall with one meter thickness and steel formwork, the concrete with low cracking sensitivity is used (MKL).

The finite element program COMET including the constitutive model developed by Cervera *et al.* (1999) is used for the simulation. The stress development during the first seven days in three different locations of the wall is investigated: the surface, the eighth of the wall and the centre. The prediction of stresses by the model is compared with the experimental results from Mangold (1994). The influence of the reference temperature, the aging and viscous effects, and the type of concrete is discussed.

4.1 Background

4.1.1 The Numerical Simulation

As described in Section 2.4, Mangold (1994) simulated experimentaly the hardening process of a concrete wall. Regarding the phenomena of the

temperature gradient three different locations in the cross-section of a wall with one meter thickness were chosen, such as the centre ($x = 0.5\,m$), the eighth ($x = 0.12\,m$) and the surface ($x = 0.0\,m$), see Figure 4.1. To simulate the hardening process each beam specimen was heated according to the temperature development in one portion of the cross-section of the wall, see Section 2.4. This temperature development was calculated in advance with a finite-element program, see Mangold (1994).

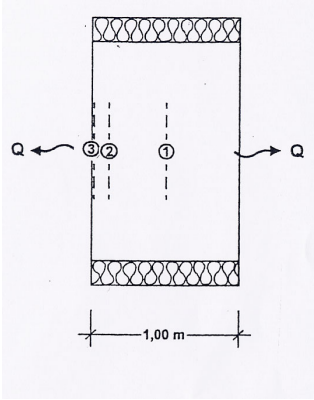

Figure 4.1: Mangold studied the Development of Stresses in the three parts of the Cross-Section of a Wall with one meter thickness: at the Centre (1), the Eighth (2) and the Surface (3).

The actual geometry, the properties and the boundary conditions of the wall which used Mangold in his finite element computation are not given in his Doctoral Thesis. However, to model this problem within the context of the finite element method a slice of the half wall with assumed conditions was first studied. The temperature development in the whole cross-section of the wall could be calculated by using the constitutive model, described in Section 3. Due to the unknown conditions of Mangold's computation, the prediction by the model developed by Cervera *et al.* (1999) did not achieve exactly the same course of temperature development.

The prediction of stresses are solved as a result of the thermal and chemical parts of the constitutive model. In order to get comparable stress results, the temperature development should be as accurate as possible. Therefore it was decided to simulate directly the "cracking-frame" experiments. The temperatures calculated by Mangold (1994) were now used as input data. A lateral slice of the beam specimen in the cracking frame is simulated in only one quadrilateral bilinear 2D element. The hypothesis of plane strain is used to simulate full restraint in the longitudinal direc-

tion; isostatic support is assumed in the transversal directions. Thus, only longitudinal normal stresses occur.

4.1.2 Relation between T_{ref} and T_{zero}

The reference temperature T_{ref} which is given in the original constitutive model developed by Cervera *et al.* (1999) is assumed to be the temperature for the transition from purely viscous to viscoelastic behaviour of the concrete, where $\xi = \xi_{set}$. Values of ξ_{set} between 0.1 and 0.4 have been proposed in various literature depending on the type of cement and the w/c ratio (Torrenti 1992; de Schutter and Taerwe 1995).

Mangold (1994) defines the behaviour of the zero-stress temperature as the temperature at which stress of restrained concrete is zero. His experimental investigations show that the zero-stress temperature highly depend on the amount and the history of temperature development.

as a matter of fact, the stress development during hydration depends on inter-related thermal, vicous and chemical aspects. In the constitutive model all aspects are considered separately while Mangold (1994) defined the zero-stress temperature from the experimental point of view, without respect to the different influencing factors. This makes it difficult to relate directly the two temperatures.

However, it is obvious that the courses of the zero-stress temperature and of the reference temperature should run parallel to each other, and both of them depend strongly on the development of the temperature in the concrete during the first days of hydration.

Therefore, as suggested by the experiments, T_{ref} is considered as an 'internal variable' of the model, to be computed at each point, in terms of the history of the local temperature during the hydration process. This means that it follows an evolution law of the type:

$$\dot{T}_{ref} = f\left(T, \dot{T}, \xi, \dot{\xi}\right) \tag{4.1}$$

or, more specifically

$$\dot{T}_{ref} = \dot{T}\, f\left(\xi\right) \tag{4.2}$$

4.1.3 Proposal for different T_{ref}

The prediction of thermally induced stresses by the model depend on thermal strain, due to thermal expansion and contraction. The amount of the thermal strain depends on the reference temperature, ($\varepsilon_T = \alpha_T(T - T_{ref})$). One objective of this work is to study the effect of the reference temperature on the stress prediction by the model. In the following numerical simulation, a changing of the reference temperatures in the program results in different stress predictions. By comparing the results, the following three equations for $\dot{T}c_{ref}$ will be discussed.

(A) The most common method used in the past was to identify T_{ref} with the initial temperature of the concrete. Which means that the reference temperature is totally independent from the development of hydration process:

$$\dot{T}_{ref(A)} = 0 \tag{4.3}$$

All parts of a cross-section have the same T_{ref} which is not consistent with the experiments.

(B) The default of the program records T_{ref} as the temperature at the end of the setting phase, (see Section 3.2.2), with $\dot{T} < \xi - \xi_{set} >$. Note that with this definition the reference temperature only depends on the single datum $\xi = \xi_{set}$, where the purely viscous behaviour of concrete changes to a viscoelastic behaviour. This change occurs in the first hours after pouring. The history of temperature development which occurs after the seeting phase is not taken into account. The result is obvious: even if the temperature development in different cross-sections differs clearly, the reference temperature is nearly the same, see Figure 4.2.

$$\dot{T}_{ref(B)} = \begin{cases} \dot{T} & if \quad \xi < \xi_{set} \\ 0 & if \quad \xi \geq \xi_{set} \end{cases} \tag{4.4}$$

(C) The experimental investigations of Mangold (1994) (see Section 2.4) show that the zero-stress temperature depends on the development of the temperature during hydration. Therefore the following equation will define the shape of the reference temperature with the variable of the hydration degree and the first derivate of the hydration temperature, such as $\dot{T}_{ref}$=$\dot{T}\, f(\dot{T}, \xi)$. Respecting the fact that the reference

temperature keeps constant at the end of the hydration phase, the following equation is proposed:

$$\dot{T}_{ref(C)} = \dot{T}\left(1 - \frac{\xi}{\xi_\infty}\right)^2 \tag{4.5}$$

Figure 4.2 helps to understand the previous definitions of the reference temperatures. The temperature development and the corresponding reference temperatures of the centre (a) and at the surface (b) of a one meter thick wall is given. Note that the development of temperature is significant different. $T_{ref(A)}$ remains constant in both cases ($T_{ref(A)} = 20\,^oC$). $T_{ref(B)}$ reaches nearly the same value at the surface and in the centre of the wall ($T_{ref(B)} \simeq 27\,^oC$). $T_{ref(C)}$ differs significantly in the two locations. The temperature development of the first days is taken into account.

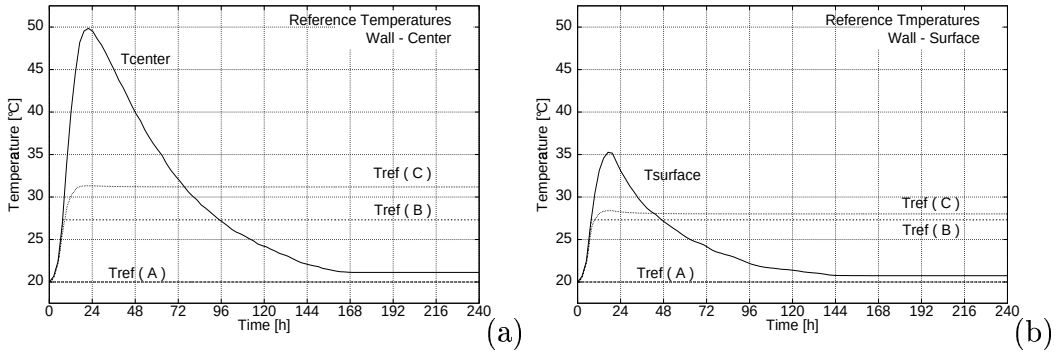

Figure 4.2: Temperature Development and the corresponding Reference Temperatures in the Centre and at the Surface of a one meter thick Wall.

4.1.4 Influencing Effects

The most important equations for the calculation of stresses are recalled here. Eq. 4.6 gives the evolution of the strain due to the viscous effect, Eq. 4.7 calculates the effective stresses of one Maxwell chain resulting from the total strain and Eq. 4.9 represents the total stresses in the concrete.

$$\dot{\boldsymbol{\varepsilon}}^i = \Big(\frac{1}{\tau^i} + \frac{1}{\tau_\mu} + \frac{1}{\tau_a}\Big)(\boldsymbol{\varepsilon} - \boldsymbol{\varepsilon}^i) = \frac{1}{\hat{\tau}^i}(\boldsymbol{\varepsilon} - \boldsymbol{\varepsilon}^i) \qquad \text{for} \quad i = 1, ..., N \tag{4.6}$$

$$\boldsymbol{\sigma}^i\left(\boldsymbol{\varepsilon}_e^i, \kappa\right) = E^i(\kappa)\,\overline{\boldsymbol{D}} : \boldsymbol{\varepsilon}_e^i \tag{4.7}$$

with

$$\boldsymbol{\varepsilon}_e^i(\boldsymbol{\varepsilon}, \boldsymbol{\varepsilon}^i, T, \xi) = (\boldsymbol{\varepsilon} - \boldsymbol{\varepsilon}_T - \boldsymbol{\varepsilon}^i - \boldsymbol{\varepsilon}_{\boldsymbol{\xi}}) \tag{4.8}$$

As the damage of concrete is not considered in this work, the stresses can be directly obtained with the following equation:

$$\boldsymbol{\sigma} \;=\; \sum_{i=1}^{N} \boldsymbol{\sigma}^i \tag{4.9}$$

Dependence on the Viscosity

The rate of viscous strain depends on the aging effect on the Young modulus (τ_a), the relaxation time of the dashpots (τ^i) and the flow term due to micro-prestresses (τ_μ). The rheological model given in Figure 4.3 describes the viscoelastic behaviour of concrete. Note that only one dashpot is introduced for the following numerical simulation. E_0 is considered as the asymptotic elastic modulus of concrete, while E^1 is the elastic modulus of the single Maxwell element in the chain. The dependence of the two elastic moduli is given with E^1=(ELAS)$\cdot E$ in the program, where $E = E^1 + E_0$. The retardation time of the dashpot, defined as $\tau^1 = \eta^1/E^1$, with the dashpot viscosity, η^1, is called RETA in the program.

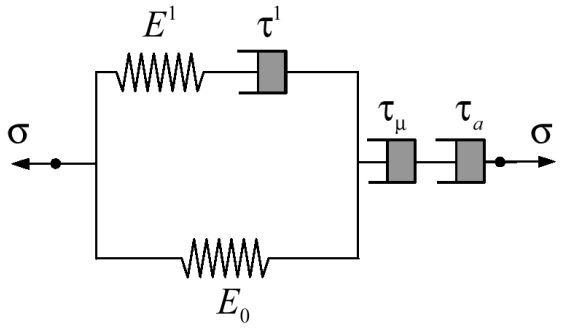

Figure 4.3: The Rheological Model for the Viscoelastic Behaviour of Concrete used for the Numerical Simulation

Aging Effect: As described in Section 3.2 the aging effect on the Young modulus is defined as $\tau_a(\kappa) = E/\dot{E}$ and occurs as long as the aging progresses and the elastic modulus varies ($\dot{E} \neq 0$). Therefore this is the most significant viscous effect in the first days ($<$ 48 hours).

Viscous Effect: The viscous effect is defined by the Maxwell chain, with E^1 and τ^1, The time of influencen depends on τ^1, but it is supposed to be the first week.

Flow Term: The flow term due to micro-prestresses (τ_μ) is introduced to account for the long term aging. Its influence occurs very much later than the previous mentioned viscous effects. As in the following numerical simulation only the first week is studied, this term is negligible.

In order to study how these different effects of viscosity influence the prediction of the stress development, the following cases will be studied and analysed. The chemical shrinkage $\boldsymbol{\varepsilon}_\xi$ can be neglected by setting its coefficient α_ξ very small.

- **Case (0):** It studies the development of stresses by elimination of all viscous effects in the Maxwell chain. The default for the calculation of the relaxation time of the total viscosity of the Maxwell chain $\hat{\tau}^i$ is given with Equation 4.6. In order to deactivate this effect of viscosity, $1/\hat{\tau}^i$ is set to zero directly in the program.

  The total stresses are calculated with Equation 4.7 and 4.9. Note that by deactivating the viscous deformations and neglecting the chemical effect the elastic strain depends only on the thermal evolution. Thermal expansion (for $T > T_{ref}$) produces compresssive stress, thermal contraction (for $T < T_{ref}$) results in tensile stresses.

- **Case (1):** The determination of the effect of viscosity, $1/\hat{\tau}^i$ is reactivated in the program. The number of Maxwell chain is set to zero, so that $1/\tau^i = 0$. Hence Case (1) consider the strain evolution depending on thermal strain and the aging effect on the elastic modulus. While thermal strains result in compressive or tensile stresses, the viscous effects only results in tensile stresses. Compressive stresses are reduced, tensile stresses increase.

- **Case (2)-(6):** They study the effect of the retardation time (RETA) and the elasticicty modulus constant (ELAS) of one Maxwell chain. To interpretate the results more easily only one Maxwell chain will be activated.

  (2) RETA: 12 h; ELAS: 0.20
  (3) RETA: 12 h; ELAS: 0.40
  (4) RETA: 24 h; ELAS: 0.20

(5) RETA: 24 h; ELAS: 0.40
(6) RETA: 10 h; ELAS: 0.25

Chemical Aspect

Mangold (1994) investigated two kinds of concretes mixed with two different cement blends. The stress development was significantly different due to the behaviour of chemical swelling and shrinkage. Therefore the coefficient of chemical shrinkage α_ξ was introduced in the following prediction.

- **Case (7):** In order to discuss the effect of chemical swelling a chemical expansion coefficient α_ξ is used ($\boldsymbol{\varepsilon}_\xi = \alpha_\xi \xi \, \mathbf{1} \, ; \alpha_\xi \leq 0$). The number of Maxwell elements in the chain was set to zero $1/\tau^i = 0$.

4.2 Calibration of the Concrete

In his experiments Mangold (1994) investigated two concretes made with cements from two differnt plants. Due to the chemical content, different cracking sensitivity could be noticed: MK-A (with a high cracking sensititvity) and MK-L (with a low cracking sensititvity).

Within a numerical simulation the first step is the calibration of the material properties. The adiabatic tests (development of temperature and Young modulus in adiabatic conditions) by Mangold (1994) gave the basis. By comparing the experimental data with the prediction by the model the material properties of both concretes could be obtained. They are listed in Table 4.1, where the second and the third blocks represent the thermal and chemical related properties, and the last one the mechanical properties.

Note that the final values of Young modulus E_∞ and the compressive

Properties	MK-A	MK-L
w/c	0.50	0.50
$\rho\ [10^3\, kg/m^3]$	2.44	2.44
$\alpha_T\ [10^{-6} K^{-1}]$	7.80	7.80
$C\ [10^6\, J/m^3\, K]$	2.53	2.53
$k_T\ [10^3\, J/m\, hs\, K]$	8.39	8.39
$T_0\ [K]$	20.0	20.0
ξ_∞	0.74	0.74
$k_\xi/\eta_{\xi 0}\ [10^6\, 1/hs]$	1.30	10.0
$\overline{\eta}$	4.80	5.90
$A_{\xi 0}/k_\xi\ [10^{-4}\,]$	1.00	9.00
$E_a/R\,[10^3\, K]$	4.00	4.70
$Q_\xi\ [10^8\, J/m^3]$	1.42	1.58
ξ_{set}	0.20	0.20
$f_\infty^-\ [N/mm^2]$	44.0	48.0
$f_\infty^+\ [N/mm^2]$	3.64	4.10
n_T	0.40	0.60
$E_\infty\ [10^3 N/mm^2]$	30.1	32.5

Table 4.1: Material Properties for the Numerical Simulations of two concretes: MK-A (high cracking sensititvity) and MK-L (low cracking sensititvity).

strength f_∞^- are higher in the concrete with a lower risk of cracking.

Calibration of MKA

The temperature development of the concrete with high cracking sensitivity (MK-A) with two different initial temperatures $T_0 = 12^oC$ and 20^oC was investigated. Figure 4.4 shows the comparison between the experiments and the prediction using the proposed thermo-chemical model. The crosses represent the experimental values; the solid line represents the prediction by the model. The properties given in Table 4.1 are the result of the calibration.

$T_0 = 20^oC$**:** The ratio E/E_∞, where E_∞ is the final value under ideal conditions is represented in Figure 4.4 a). Note that the development of Young modulus is nearly exactly reproduced. In Figure 4.4 b) the temperature rise versus time is given. It was not possible to reproduce accurately the same development of temperature as the given results from adiabatic tests by Mangold (1994). Note that the hydration of the calibrated con-

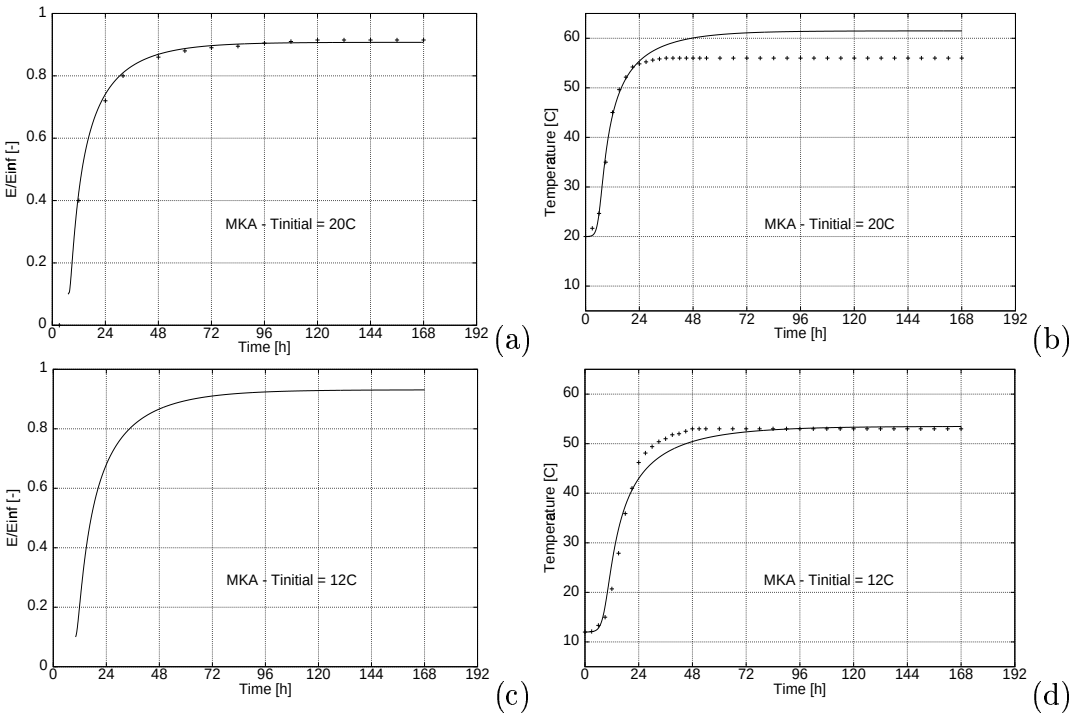

Figure 4.4: Development of Temperature and Young modulus in Adiabatic Conditions of the Concrete with high Cracking Tendency (MKA). Results of the Adiabatic Tests by Mangold (+) and the Prediction by COMET (-).

crete takes about three days until the process is finished. The final value of Young modulus of the experimental investigated concrete is also achieved after three days, while the temperature rise nearly stops to increase after one day. This phenomenon is incompatible with the basic assumption of the model. This discrepancy is attributed to heat losses in the experimental settings.

$T_0 = 12^oC$**:** The ratio E/E_∞ predicted by the model is represented in Figures 4.4 c). Experimental results are not given. The temperature prediction with an initial temperature of $T_0 = 12^oC$, see Figures 4.4 d), catches nearly exactly the experimental results.

The development of Young modulus is nearly exactly reproduced during the first seven days. As already explained in the previous chapter, the hydration during the first day is highly important. In both conditions the development of temperature during the first day is represented quite well. Note that, starting with different initial temperature T_0, the model can not predict a different $(\Delta T)_{adiabatic}$ in adiabatic conditions, while in the adiabatic tests by Mangold a significant difference of $(\Delta T)_{adiabatic} = 5\,^oC$ occured.

Calibration of MKL

The concrete with low cracking sensitivity (MK-L) is now calibrated. The cement of MKL has a lower alkali content (K_2O, Na_2O) than MKA. Breitenbücher (1994) proved that these cements lead to a low temperature

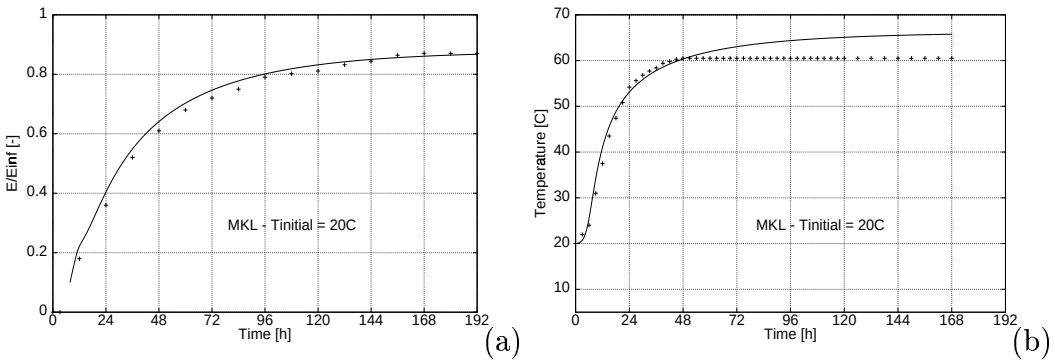

Figure 4.5: Development of Temperature and Young modulus in Adiabatic Conditions of the Concrete with low Cracking Tendency (MKL). Results of the Adiabatic Tests by Mangold (+) and the Prediction by COMET (-).

development and a slower development of the Young-modulus and the tensile strength.

$T_0 = 20^oC$**:** The ratio E/E_∞ in 4.5 a) represents this phenomenon. Its prediction is nearly perfect. Figure 4.5 b) shows the temperature rise versus time. The final temperature could not be represented exactly. More heat than in the adiabatic test by Mangold (1994) is produced. However, during the first two days the course of the development of temperature could be represented quite well. Note that the development of temperature in the adiabatic test by Mangold (1994) is slower but the final value is about 3^oC higher than in MKA.

4.3 Case Study 1: Steel Formwork - MKA

The following numerical simulations shows the prediction by the model of the stress development in three elements according to the three parts of the cross-section of the wall, the centre, the eighth and the surface. The stress prediction is made starting from a given development of temperature by Mangold (1994). In order to understand the effects of different reference temperatures on the development of stresses, each prediction will be carried out with the three proposed equations for the reference temperature, see Section 4.1.3. Furthermore the stress calculation will be made with different viscous effects.

4.3.1 Development of Temperature

Figure 4.6 shows the development of temperature during the first seven days of hydration in the three investigated parts of the $1.0\,m$ thick cross-section.

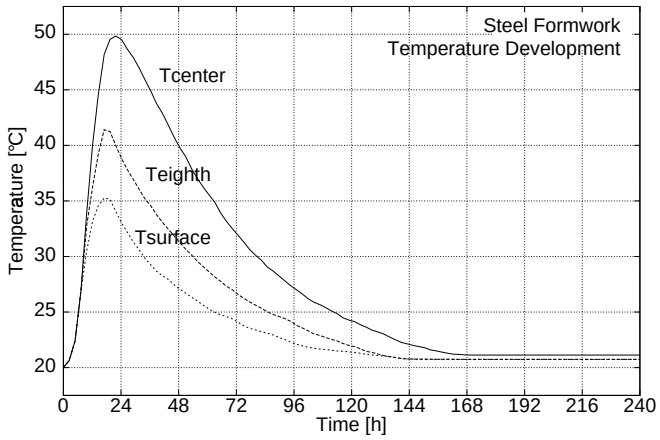

Figure 4.6: Case Study 1: Development of Temperature by Mangold (1994) in the three Parts of the Cross-section of the Wall, the Centre ($x = 0.5m$), Eighth ($x = 0.12m$) and Surface ($x = 0.0m$).

The corresponding reference temperatures are calculated by COMET. According to the temperature development, they are represented in Figure 4.7 b) to 4.7 d). The different calculations were made with Eq. 4.3, Eq. 4.4 and Eq. 4.5, proposed in Section 4.1.3.

(A) In all parts of the cross-section $T_{ref(A)}$ is equal to the initial temperature, ($T_{ref(A)} = 20\,^oC$).

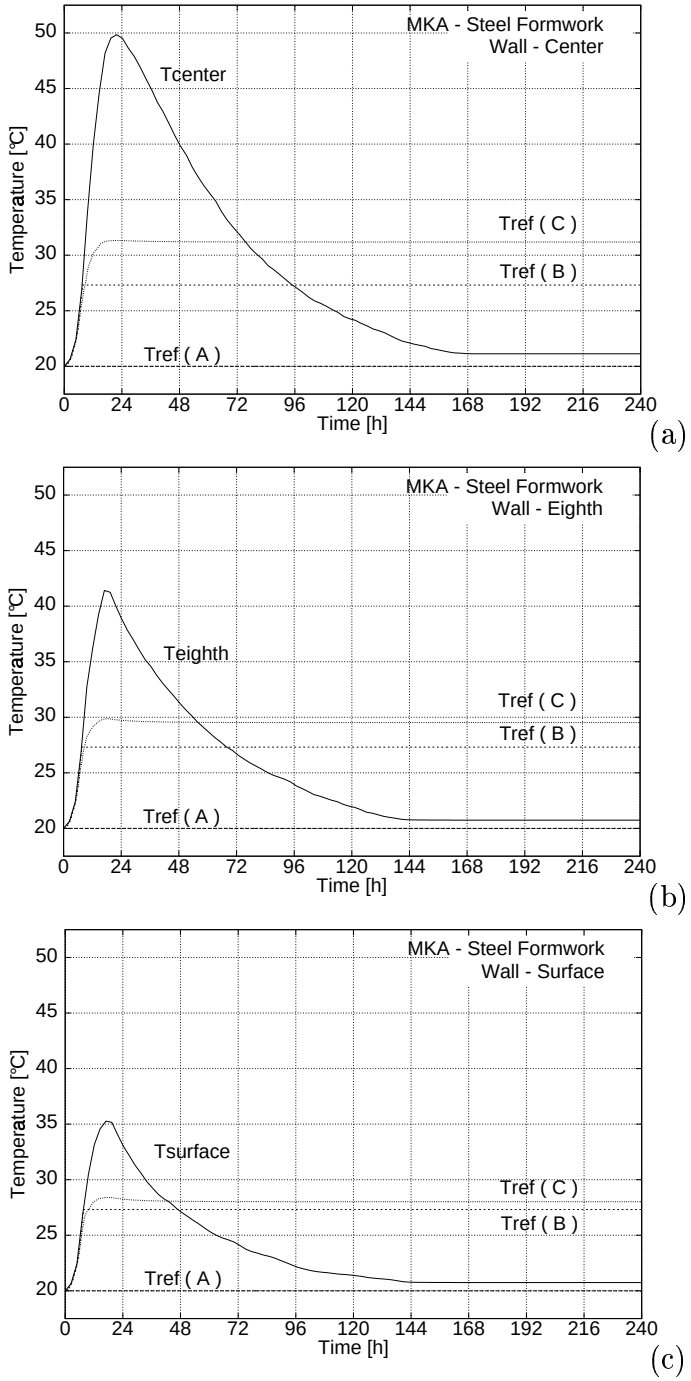

Figure 4.7: Case Study 1: Development of Temperature by Mangold (1994) and the corresponding Reference Temperatures calculated by COMET in Elements according to the three Parts of the Cross-section of the Wall, the Centre ($x = 0.5m$), Eighth ($x = 0.12m$) and Surface ($x = 0.0m$).

(B) $T_{ref(B)}$ only depends on the actual temperature when the transition from purely viscous to viscoelastic behaviour of the concrete takes place (where $\xi = \xi_{set}$). As the development of temperature in the different cross-sections of the wall during the first hours does not differ signifcantly, $T_{ref(B)}$ reaches approximately the same final value ($T_{ref(B)} \simeq 27\,^oC$).

(C) $T_{ref(C)}$ increases until the maximal amount of temperature is reached. Then it remains nearly constant. The temperature difference between the different parts of the cross-section are:

- $\Delta\, T_{ref(C)} \sim 1.5\,^oC$ between the centre and the eighth;
- $\Delta\, T_{ref(C)} \sim 2\,^oC$ between the eighth and the surface of the wall.

4.3.2 Development of Stresses

As already explained in the previous pages, the numerical simulation of stress development regarding the influence of different reference temperatures and the effects of viscosity will be discussed. The comparison between the influencing factors, proposed in cases (0) to (6), see Section 4.1.4, will be carried out.

Figure A.2 show the development of the stresses locations of the cross-section when the viscous effect was deactivated, see Case (0) in Section 4.1.4. Note that negative stresses are compressive stresses, and positive are tensile stresses. The influence of the reference temperature is directly recognizable. Thermal expansion, where $\varepsilon_T = \alpha_T(T(t) - T_{ref}) \geq 0$, results in compressive stresses. Tensile stresses due to thermal compression only occur when using $T_{ref(B)}$ or $T_{ref(C)}$, but they are clearly underestimated. This means that viscous effects are essential to represent the real behaviour during these first hours.

Case (1) is represented in Figure A.3. The development of stresses is now predicted regarding the viscous effects due to the flow term and the aging of the Young modulus. The effects of different reference temperatures can hardly be noticed anymore. In the first 20 hours the stresses $\sigma_{Tref(A)}$, $\sigma_{Tref(B)}$ and $\sigma_{Tref(C)}$ increase differently, but after reaching the maximum value the courses remain parallel and they hardly differ ($\sigma_{Tref(C)} - \sigma_{Tref(A)} \leq 0.5 N/mm^2$). In all investigated elements the experimental measured stresses develop slowlier than the numerical simulation predicts. The

best representation of the stresses is obtained using $T_{ref(C)}$. In all the three simulated sections the maximum compressive stress is predicted nearly exactly with $\sigma_{Tref(C)}$. The prediction at the surface corresponds to the real development during all the seven days. The final tensile stresses is almost exactly achieved. In the other simulated parts of the cross-section the predicted tensile stresses are overestimated. This means that the aging effect is the dominant viscous effect during the first 24-48 hours but it disappears almost completely afterwards and additional viscous mechanisms must be considered in the model.

For the following cases (2) to (5) dashpot constants defining the retardation time RETA and the Young modulus constant ELAS of the Maxwel chain are introduced, see Figure4.10. In order to do an accurate interpretation of the results the simulation is carried out by using only one Maxwell chain. The three proposed reference temperature are used. Once again, the best representation of the stresses is obtained using $T_{ref(C)}$.

Therefore the results of the cases (2) to (5) only using $T_{ref(C)}$ are shown in Figure 4.11. By comparing the results the effect of the retardation time (RETA) and the elasticity modulus constant (ELAS) can be studied. Figures a) to c) shows the simulation of Case (2) and (3) with RETA: 12 hours and ELAS: 0.2 and 0.4. In Figures d) to f) Case (4) and (5) with RETA: 24 hours and ELAS: 0.2 and 0.4 are studied. The longer the retardation time, the more time needs the dashpot to react. This phenomena can be observed in Figure 4.11 by comparing the simulations on the left side with the simulations on the right side. The compression in the concrete decreases later and thus a loss of tensile stresses occurs later.

The evolution of the stress in the element with a higher temperature, (the centre), is exactly predicted with 12h and 0.4. For the element in the eighth of the wall an exact simulation would be find between 0.2 and 0.4 with the retardation time of 12h. The introduction of the dashpot at the surface does not improve the results. A constant value of dashpot viscosity, which fulfills all investigated sections perfectly does not exist, but to define a compromise the following values are choosen: ELAS$\sim$ 0.3 and RETA: 12 hours.

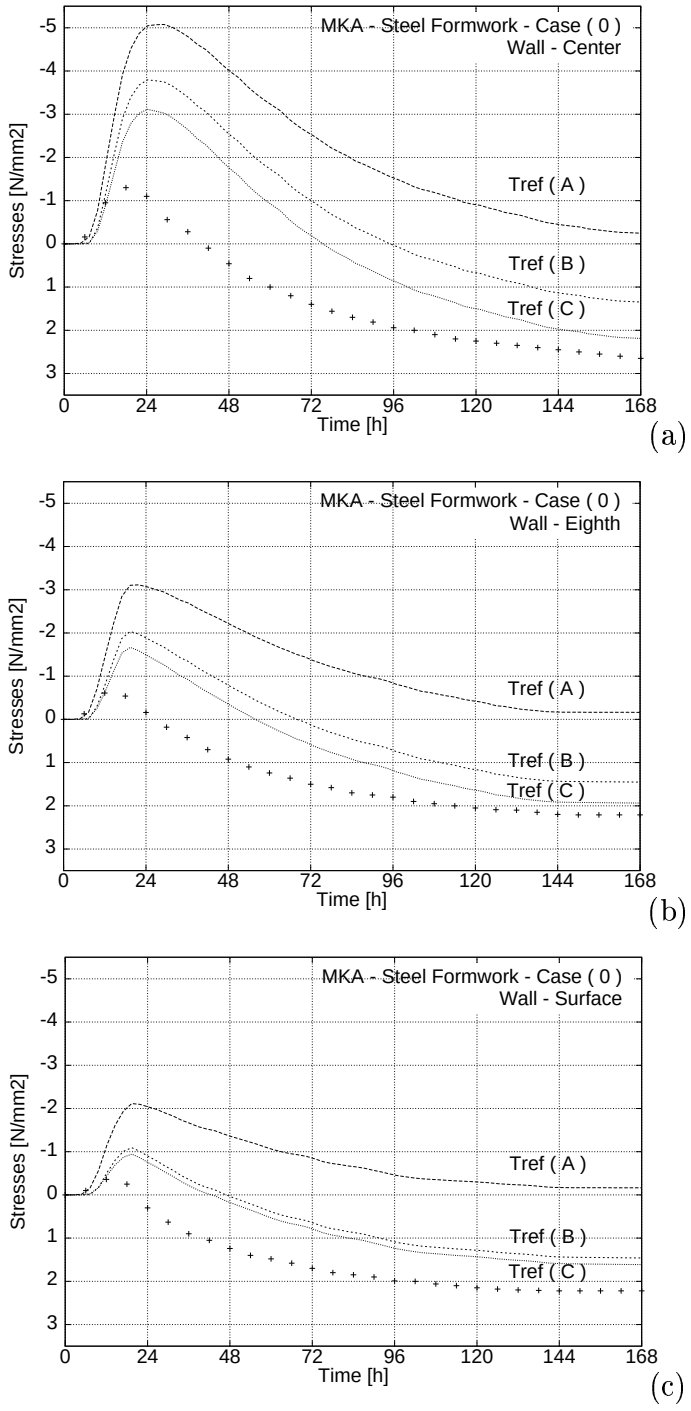

Figure 4.8: Case Study 1: Numerical Simulation of the Stress Development in the wall without any Viscous Effect.

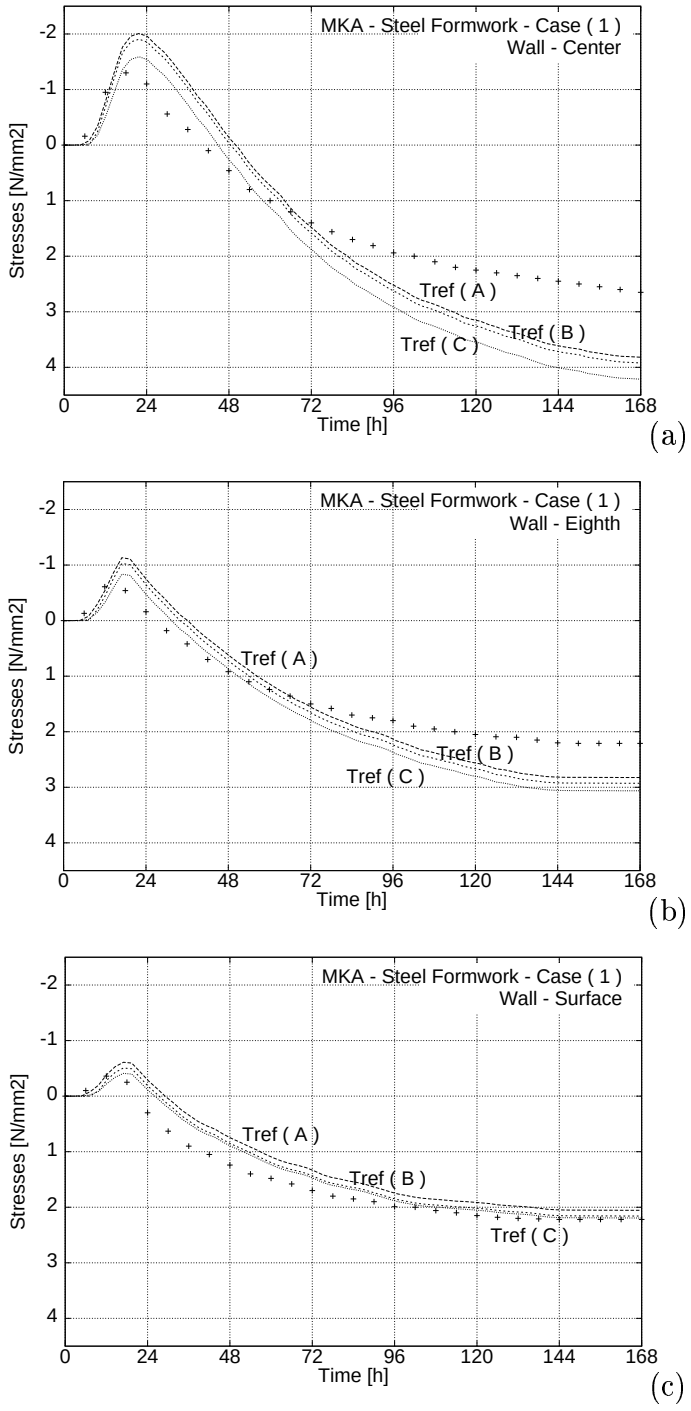

Figure 4.9: Case Study 1: Numerical Simulation of the Stress Development in the wall regarding the Viscosity.

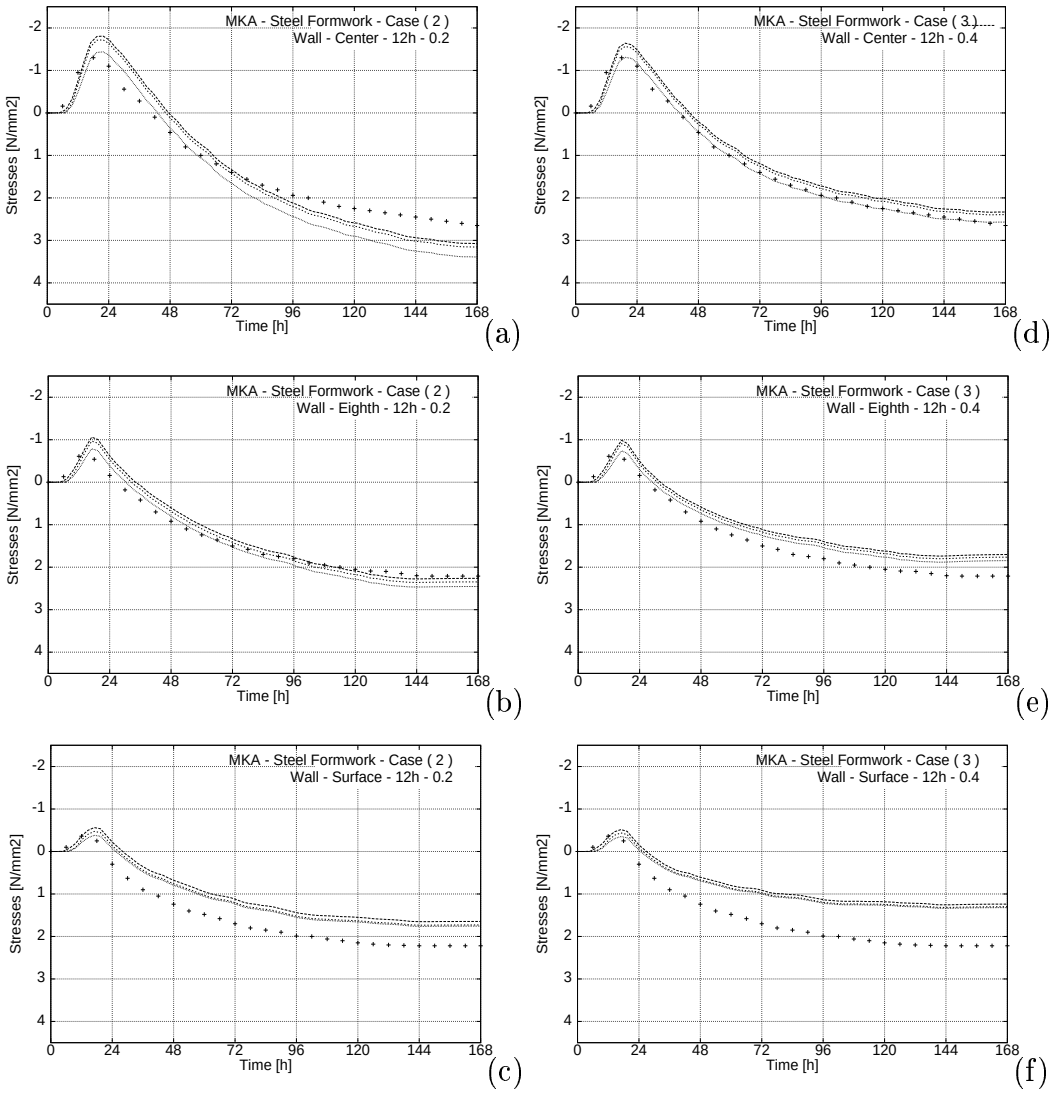

Figure 4.10: Case Study 1: Numerical Simulation of the Stress Development in the wall with RETA:12h, ELAS:0.2 (Figure a) to c)) and RETA:24h, ELAS:0.4 (Figure d) to f)). All predictions are made with $T_{ref(A)}$,$T_{ref(B)}$,$T_{ref(C)}$ and with the MKA Concrete.

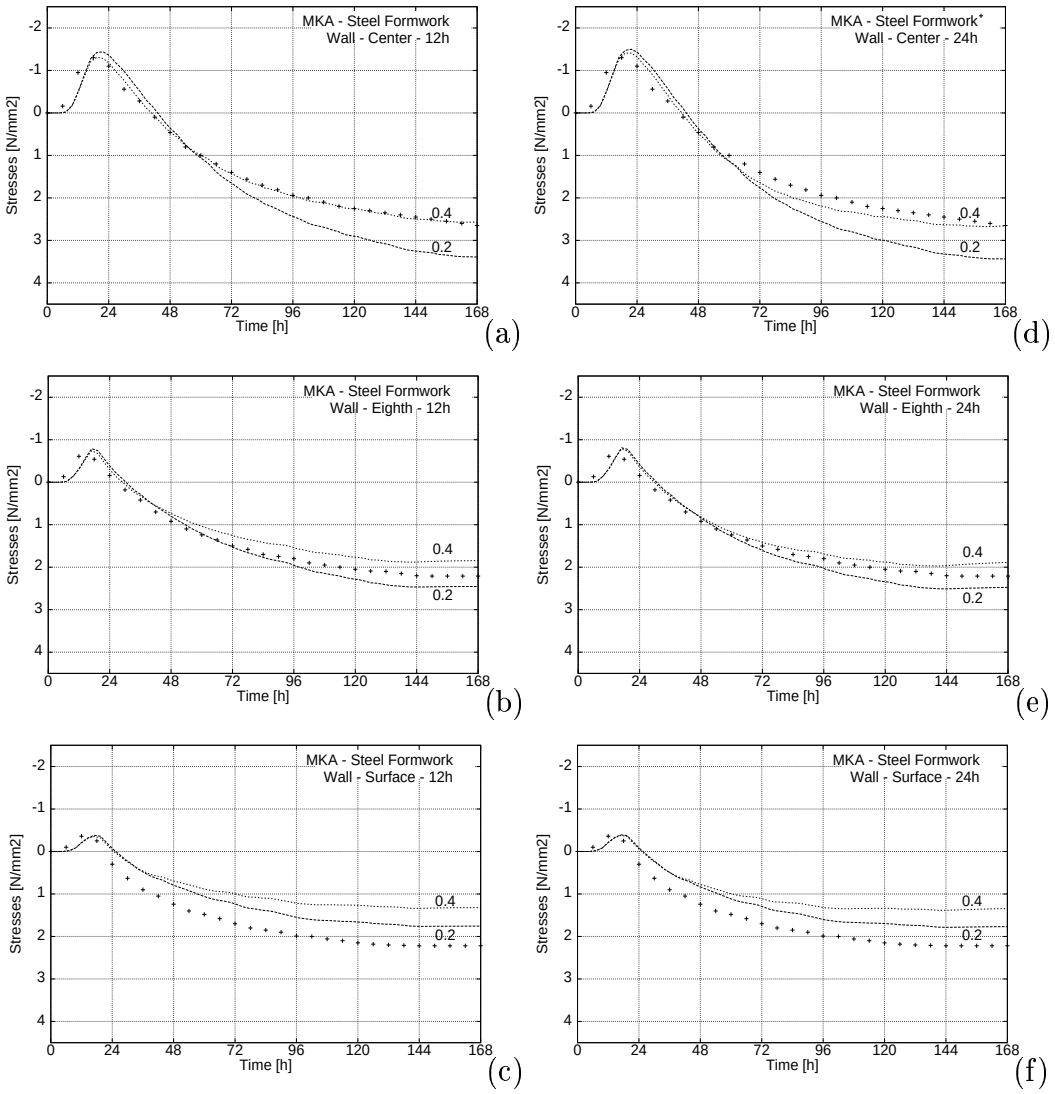

Figure 4.11: Case Study 1: Numerical Simulation of the Stress Development in the wall with RETA:12h (Figure a) to c)) and RETA:24h (Figure d) to f)). All predictions are made with $T_{ref(C)}$ and with the MKA Concrete.

4.3.3 Conclusion

The numerical simulation of **Case Study 1** (the stress development in a wall with a steel formwork) allows the following three conclusion about the reference temperature, the effect of aging (variable Young modulus) and viscosity:

- **Reference Temperature:** The thermal strains depend on the definition of the reference temperature. By using the constitutive model these strains are almost superseded by strains due to the viscous effects. Hence the different choice of reference temperatures does not influence the results significantly. But as already remarked in Case (1) the numerical simulation using $T_{ref(C)}$ delivers the best fittings of on the experimental results. As this reference temperature depends on the development of temperature is the most reliable. The whole history of hydration is taken into account. Therefore $T_{ref(C)}$ is fixed with Eq. 4.5 in the constitutive model and all the following simulation will be carried out by using the reference temperature $T_{ref(C)}$.
- **Aging Effect:** The aging effect is essential and occurs as long as the aging progresses and the elastic modulus varies. It is dominant during the first 24-48 hours, where most of the aging takes place.
- **Viscous Effect:** The development of stresses during the first day is almost independent from the dashpot viscosity. This is obvious as the dashpot delays the process and needs time to start its reaction. With the retardation times $\tau^i \geq 12$h the beginning of the dashpot influence occurs after the first two days.

  In order to achieve an exact prediction of the stress development in all the investigated parts of the cross-section of the wall, different dashpot viscosities are necessary. The smaller the temperature development the less viscous the concrete behaves. Thus at the surface (where the temperature is low) the viscous effects are neglectable, while they help to improve the results in the eighth and in the centre of the wall (where the temperature is much higher). This means that the viscous effect of the dashpot depends on the temperature.

  Furthermore, it was found out that the shorter the retardation time the better the experimental results are fitted. Thus the viscous effect of the dashpot is already significant in the first days of hydration.

The definition of the dashpot viscosity is involved in the calibration of the material properties. Once the retardation time and the elasticity modulus constant is fixed, all the prediction are made with this calibrated concrete. With the average values of RETA and ELAS, the tensile stresses according a high development temperature (such as in the centre of a wall) will be overestimated, and the tensile stresses according a low development temperature (such as at the surface of a wall) are underdestimated. The over- and underdestimation amounts to less than $\Delta\sigma \sim 0.6\,N/mm^2$, which is about 1/6 of the tensile strength ($f_\infty^+ = 3.64 N/mm^2$).

4.4 Case Study 2: Wooden Formwork - MKA

In order to verify the applicability of the conclusions previously given, the case study of a wall with a hindered heat transfer will be numerically simulated. The same MKA concrete will be investigated.

4.4.1 Development of Temperature

Constructing a wall with a wooden formwork, the heat production and thus the temperature development is significantly higher than in a wall builded with a steel formwork. Besides the heat loss is much slower. After two days the formwork is stripped and then the temperature decreases rapidly at the surface decreases and slowly in the centre and in the eighth. Due to the hindered heat transfer the temperature development in the centre and at the eighth of the wall is nearly the same. Th maximum temperature at the surface is about $8\,^oC$ higher than in Case study 1. Figure 4.12) shows the development of temperature during the first seven days of hydration according to the three investigated sections of an one meter thick wall ($x = 0.5\,m$; $0.12\,m$; $0.0\,m$).

The corresponding reference temperatures are calculated by COMET, they are represented in Figures 4.13 a) to 4.13 c). Note that we now only present the reference temperature $T_{ref(C)}$ as it proved to be the most reliable

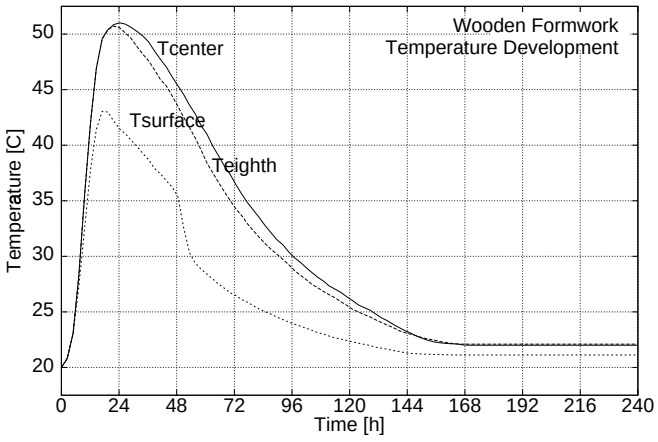

Figure 4.12: Case Study 2: Development of Temperature by Mangold (1994) in the three Parts of the Cross-section of the Wall, the Centre ($x = 0.5m$), Eighth ($x = 0.12m$) and Surface ($x = 0.0m$).

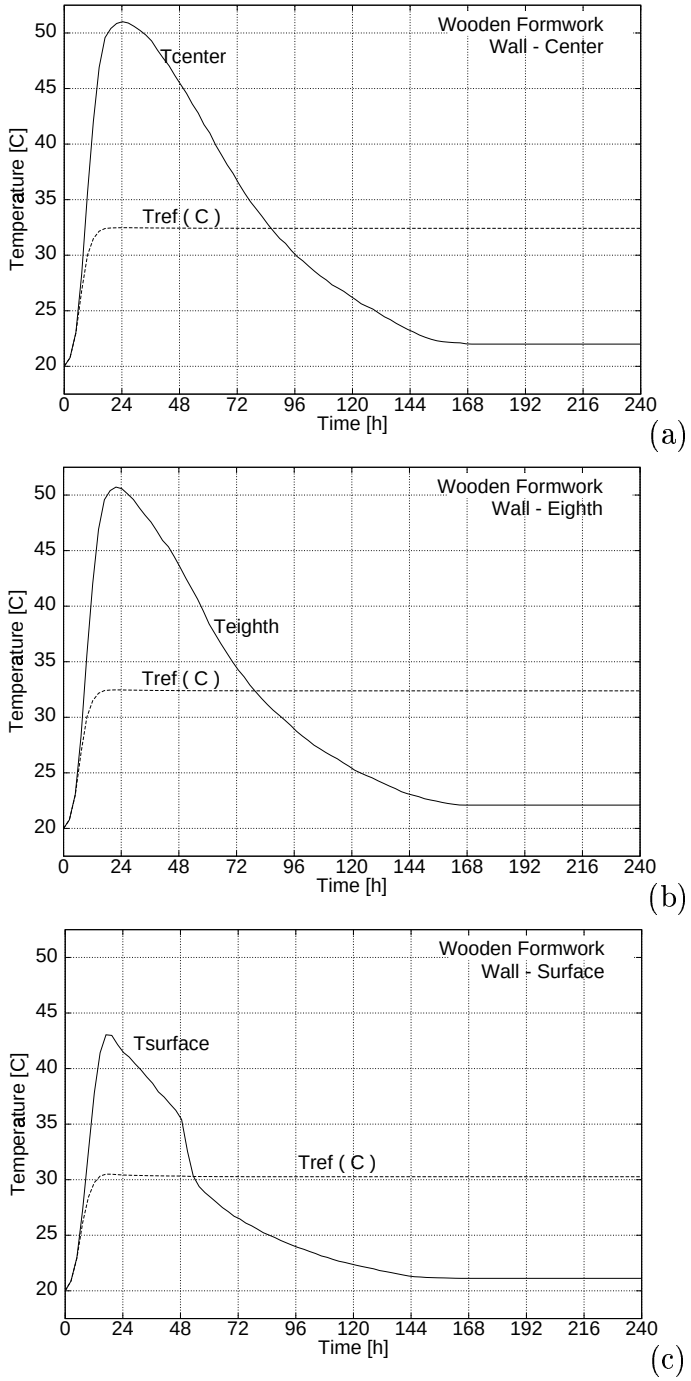

Figure 4.13: Case Study 2: Development of Temperature by Mangold (1994) and the corresponding Reference Temperature calculated by COMET in three Elements according to the three Parts of the Cross-section of the Wall, the Centre ($x = 0.5m$), Eighth ($x = 0.12m$) and Surface ($x = 0.0m$).

definition with the best results. Due to the higher temperature development in walls with hindered heat transfer in the first two days, the reference temperature of the different locations is much higher than in Case 1. Note that the temperature difference between the centre and the eighth is now negligible, between the eighth and the surface $\Delta T_{ref(C)}$ is about $3\,^oC$.

4.4.2 Development of Stresses

Figure 4.14 demonstrates that the same phenomena which were found in the first case study are fulfilled. The higher the development of temperature the more important is the viscous effect in the concrete. Furthermore, a short retardation time helps again to approach the experimental results quite perfectly. By using the retardation time of 24 hours the viscous effect starts too late, and thus the tensile stresses in the first five days are overestimated.

By using a formwork with a hindered heat transfer we notice that the temperature development in the centre and in the eighth is nearly the same. Therefore nearly the same viscous effect for both parts of the cross-section is needed. A good calibration is achieved with using ELAS between 0.4 and 0.6 and RETA $\leq$ 12 hours. The development of stresses at the surface is predicted closely by choosing ELAS between 0.2 and 0.4 and RETA:12 hours. Note that the temperature at the surface is higher than in Case Study 1. Therefore the dashpot viscosity is needed.

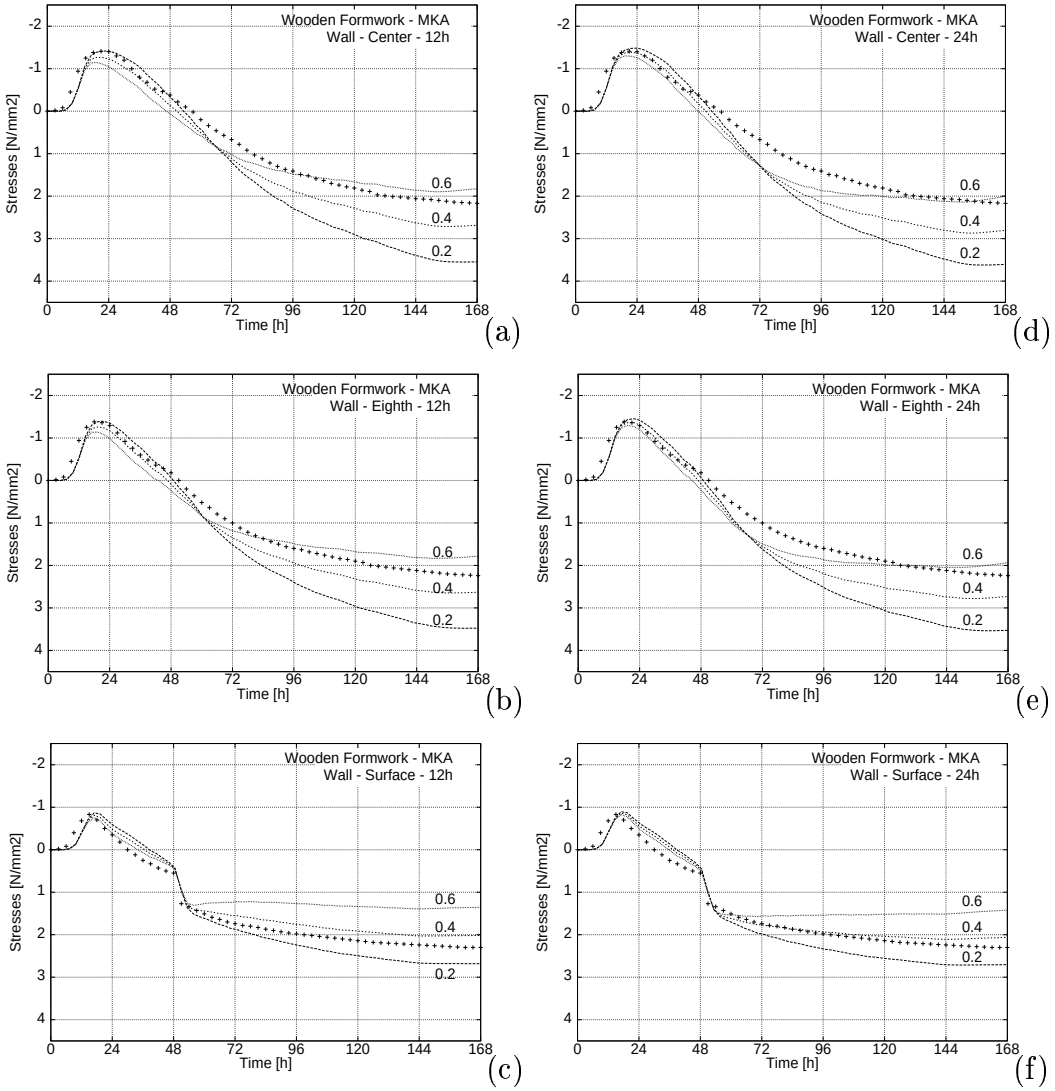

Figure 4.14: Case Study 2: Numerical Simulation of the Stress Development in the wall with RETA:12h (Figure a) to c)) and RETA:24h (Figure d) to f)). All predictions are made with $T_{ref(C)}$ and with the MKA Concrete.

4.4.3 Conclusion

The numerical simulation of **Case Study 2** (the stress development in a wall with a wooden formwork) allows the same conclusions regarding the effect of aging (variable Young modulus) and viscosity as in Case Study 1.

- **Aging Effect:** The aging effect is essential and occurs as long as the aging progresses and the elastic modulus varies. It is dominant during the first 24-48 hours, where most of the aging takes place.
- **Viscous Effect:** The development of stresses during the first day is almost independent from the dashpot viscosity. This is obvious as the dashpot retards the process and needs time to start its reaction. With the retardation times $\tau^i \geq 12$h the beginning of the dashpot influence occurs after the first two days.

  Once again, different dashpot viscosities are necessary in order to achieve an exact prediction of the stress development in all the investigated parts of the cross-section of the wall. The smaller the temperature development the less viscous the concrete behaves. Thus at the surface (where the temperature is low) the viscous effects are neglectable, while they help to improve the results in the eighth and in the centre of the wall (where the temperature is much higher). Which means, that the viscous effect of the dashpot depends on the temperature.

  Furthermore it is also shown that the shorter the retardation time the better the experimental results are approached. Thus the viscous effect of the dashpot is already significant important in the first days of hydration.

  Note that the heat production in this Case Study 2 (a hindered heat transfer during the first two days) is significantly higher than in Case Study 1. As a result the temperature development in all locations of the wall is much higher, thus the vicous effect is more important.

4.5 Case Study 3: Steel Formwork - MKL

The numerical simulation of the following case study helps to verify the prediction of a concrete with a different type of cement mix. The concrete previously studied(MKA) and this concrete (MKL) differ in their cracking tendency. As already explained in Section 4.2 the cracking tendency of MKL is much lower. Due to the so called "low heat cement" with a slow development of Young's modulus and tensile stregth, the cracking temperature is much lower, see Section 2.4. The process of hydration is much slower and the final tensile strength is higher.

4.5.1 Development of Temperature

Breitenbücher (1994) proved for low-alkali cements that a low alkali content (K_2O, Na_2O) and high sulphate content related to C_3A lead to a low temperature development and thus a low cracking temperature. Besides the development of the Young-modulus and the tensile strength is slower. Therefore the maximum temperature of MKL is expected to occur later and to be lower than in the first Case study, using the MKA. Figure 4.15) shows the development of temperature during the first seven days of hydration. Comparing this case study with the Case Study 1, the temperature maximum really occurs later in all studied locations (about eight hours later). But the maximum temperature in the centre is about one degree higher

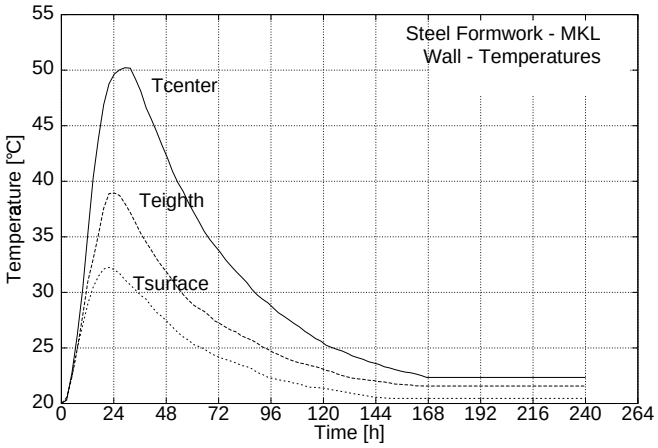

Figure 4.15: Case Study 3: Development of Temperature by Mangold (1994) in three Parts of the Cross-section of the Wall, the Centre ($x = 0.5m$), Eighth ($x = 0.12m$) and Surface ($x = 0.0m$).

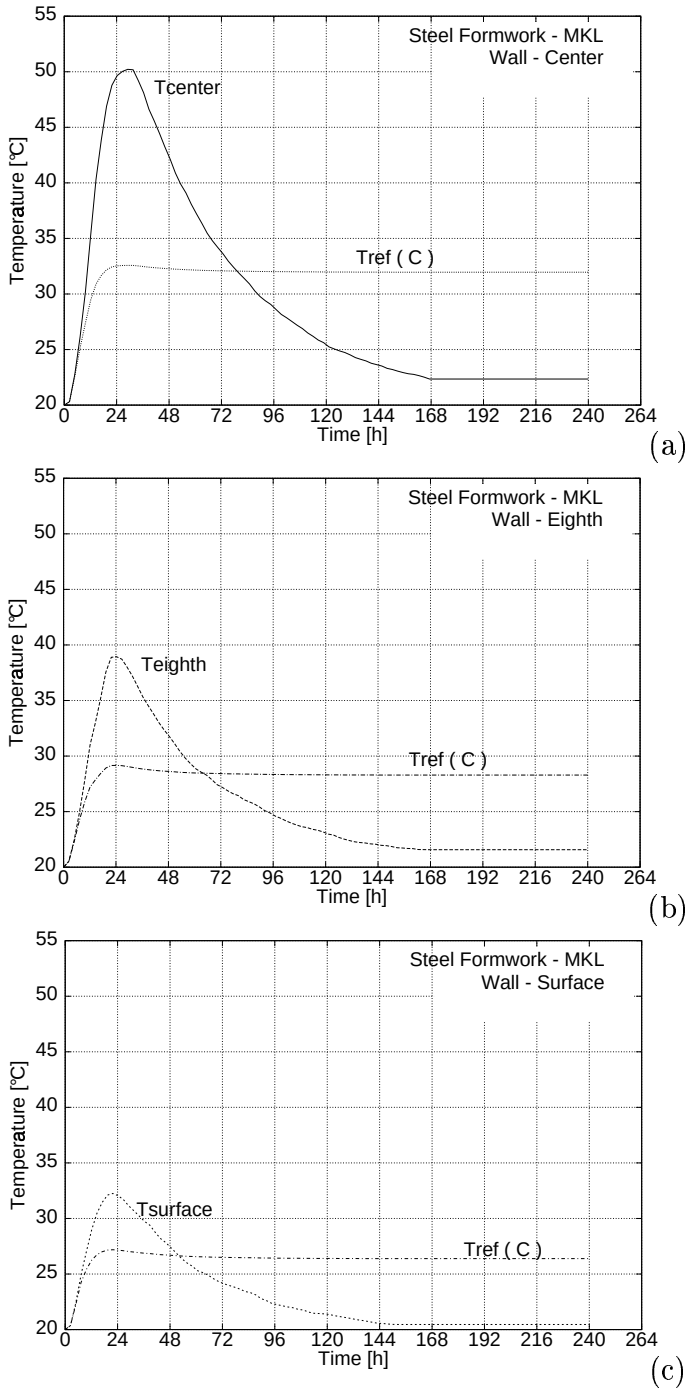

Figure 4.16: Case Study 3: Development of Temperature by Mangold (1994) and the corresponding Reference Temperatures calculated by COMET in Elements according to the three Parts of the Cross-section of the Wall, the Centre ($x = 0.5m$), Eighth ($x = 0.12m$) and Surface ($x = 0.0m$).

than in the first Case study, while the temperature at the surface and in the eighth become smaller, as expected.

The corresponding reference temperatures are shown in Figures 4.16 a) to 4.16 c). As the temperature maximum in the centre occurs nearly ten hours later and is about one degree higher than in the first Case study the reference temperature is higher. Due to the lower temperature development in the eighth and at the surface, using MKL the reference temperature of this locations is much lower than in Case 1.

4.5.2 Development of Stresses

The results of this numerical simulation verify the the dependence of the viscous effect on the temperature. The higher the temperature development the more significant the effect of viscosity.

The final amounts of tensile stresses in the eighth of the wall are predicted nearly perfectly without using any dashpot. While the compressive stresses during the first two days are underestimated by the prediction, see Figure A.16 b). As explained in Section 2.4 the different chemical composition of the cement influences the behaviour of chemical swelling. By introducing a chemical expansion coefficient α_ξ, chemical swelling is activated (7). A more significant chemical swelling at the beginning and thus a better prediction of compressive stresses are the results. Even if the stress prediction during the first days can be improved, the chemical swelling worsen the tensile stress prediction.

The final values of tensile stresses in the centre of the wall can be nearly achieved using a dashpot defined by RETA:10h and ELAS:0.25. The development of compressive stresses takes more time than in the experiments. The maximum value of compressive stress could be nearly achieved, see Figure A.16 a).

The final values of tensile stresses in the eighth of the wall are predicted nearly perfectly without using any dashpot (ELAS:0.0). However the compressive stresses during the first two days are underestimated by the prediction, see Figure A.16 b).

In all the studied cases the final values of tensile stresses at the surface of the wall are underestimated by the prediction, even if ELAS:0.0. The introduction of the chemical swelling worsens the results. The maximum value

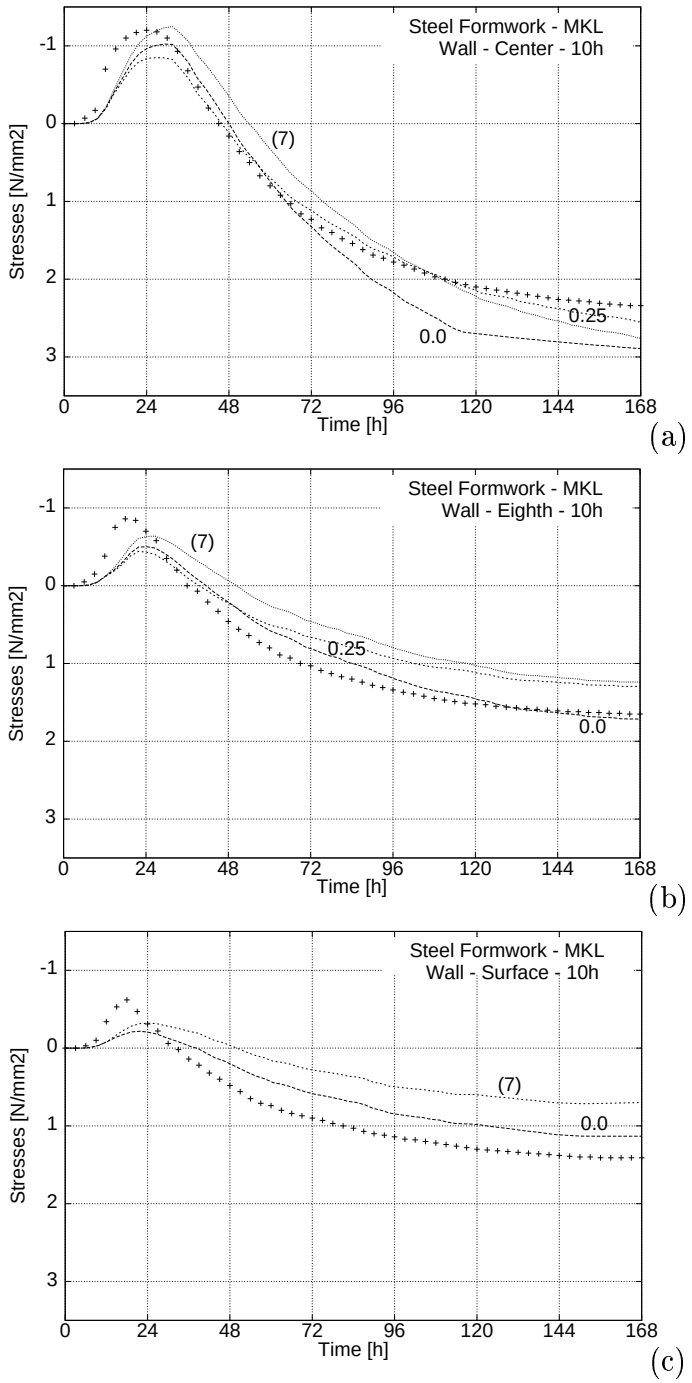

Figure 4.17: Case Study 3: Numerical Simulation of the Stress Development in the wall with different viscous effects (RETA:10h, ELAS:0.0 and RETA:10h, ELAS:0.25) and the introduction of chemical swelling (7). All predictions are made with $T_{ref(C)}$ and with the MKL Concrete.

of compressive stress is improved, but still the stresses are underestimated, see Figure A.16 c).

4.5.3 Conclusion

The numerical simulation of **Case Study 3** (the stress development in a wall with a steel formwork and the MKL concrete with low cracking tendency) allows the same conclusions regarding the effect of viscosity as in Case Study 1 and 2. Besides the effect of chemical shrinkage/swelling can now be interpreted.

- **Aging Effect:** As it is already shown in Case Study 1 and 2, the aging effect is dominant during the first 24-48 hours, where most of the aging takes place.
- **Viscous Effect:** Once again it could be shown that the development of stresses during the first day is almost independent from the dashpot viscosity and that the smaller the temperature development the less viscous the concrete behaves.
- **Chemical Aspect:** By introducing a chemical expansion coefficient α_ξ a more significant chemical swelling at the beginning can be achieved. Thus the compressive stress prediction increases and the beginning of tensile stresses starts later. This is the infavourable consequence of the chemical swelling. The tensile stresses are underestimated.

  The cement of this "low-cracking temperature" concrete MKL has a different chemical behaviour than ordinary Portland cements (such as MKA) due to a lower alkali content (K_2O, Na_2O). This lead to lower hydration heat and slower strength and stiffness evolution. This would account for the poor quality of the calibration. The actual model is not fully adequate for this sort of cement mixes. However, it can be noticed, that the higher the temperature development the better the course of the stress development can be achieved. The model represents the element in the centre nearly perfectly.

Chapter 5

Conclusion and Future Work Lines

Hydration and thus the development of the temperature in young concrete is a highly complex process. Hydration heat and the resulting stresses are not only very important for massive concrete constructions but also for members about 30 cm thick and more.

This work includes the numerical simulation of different locations within one meter thick walls experimentally investigated by Mangold (1994). Mangold simulated the hardening process in different walls during the first seven days with the help of a so called "cracking frame". Continuous measurings of deformations gave the basis to quantify the stresses and thus the zero-stress temperature in the studied locations.

The aim of the work is to verify the prediction of stress development of the finite element program COMET including the constitutive model, developed by Cervera *et al.* (1999). The reference temperature used for the calculation of thermal strains in the model is discussed in relation to the zero-stress temperature given by Mangold (1994). Moreover the effect of viscosity and the chemical aspect of the model are studied. Starting from a given development of temperature from Mangold (1994), all parts of the cross-section could be simulated in one element. The predicted stress development is compared with the experimental results of Mangold (1994).

5.1 Conclusion

The following conclusions regarding the reference temperature, the effect of viscosity, and the chemical problem can be pointed out:

Reference Temperature: Thermal strains are calculated from the temperature difference between the actual concrete temperature and the reference temperature. Different definitions of reference temperatures for the model are proposed in this work. Using the constitutive model these strains are almost superseded by strains due to the viscous effects. Hence the definition of the reference temperature does not influence the results significantly. However, the numerical simulation using a reference temperature which depends on the temperature development in each location $T_{ref(C)}$ delivers the best approaches on the experimantal results. As this reference temperature takes the whole history of hydration into account, it is the most reliable. Therefore it is suggested to fix this definition, $T_{ref(C)}$ see Chapter 4, in the constitutive model.

Effect of Viscosity: In the constitutive model developed by Cervera *et al.* (1999) the following two viscous effects are considered to occur in the first week of hydration:

- Aging Effect: The aging effect is essential and occurs as long as the aging progresses and the elastic modulus varies. It is dominant during the first 24-48 hours. The representation of the stresses for ordinary Portland cements, such as MKA, during these first days is almost perfect.

- Viscous Effect: In order to achieve an exact prediction of the stress development after the first day an additional viscous effect is introduced. It is defined by the dashpot viscosity of the Maxwell chain, which is used in the model. It is found that the shorter the retardation time of this dashpot the better the agreement with the experimental results. Which means that the viscous effect of the dashpot is important in the first days of hydration.

In order to achieve an exact prediction in all the investigated locations of the wall, different dashpot viscosities are necessary. The smaller the temperature development the less the viscous behaviour of concrete. Thus at the surface (where the temperature is low) the viscous effects are negligible, while they help to improve the results in locations with higher temperature. This means that the viscous effect of the dashpot depends on the temperature.

- Chemical Problem: The cement of this "low-cracking temperature" concrete MKL has a different chemical behaviour than ordinary Portland cements (such as MKA) due to a lower alkali content (K_2O, Na_2O). This leads to lower hydration heat and slower strength and stiffness evolution. This accounts for a poorer quality of the calibration. The actual model is not fully adequate for this sort of cement mixes. However, it can be noticed that the higher the temperature development the better the course of the stress development can be achieved. The model represents the element with a high temperature development and this concret MKL almost perfectly.

5.2 Future Work Lines

The conclusions show that further investigations would be helpful to understand the effects of the reference temperature, the viscosity, and the chemical problem more exactly:

Reference Temperature: As it is demonstrated, the reference temperature is not as important for the stress prediction by the constitutive model as expected. Thermal stresses are mainly superseded by stresses due to viscous effects. Anyhow, in order to respect the history of temperature in the member, it is suggested to change the actual definition of the reference temperature used in the constutive model by Cervera (1999). The proposed definition is given in Chapter 4.

Effect of Viscosity: One of the main results of this work is the realisation that the dashpot viscosity depends on the temperature. This phenomena should be deeperly studied with the help of further experiments. The question of how grave the inexact stress prediction and the effects on real concrete construction should be assessed. The fact that this work only studies the first seven days of hydration makes it recommendable to estimate the influence in older concrete.

Chemical Problem: The numerical simulation shows that an exact representation by the constitutive model of a concrete with low cracking tendency is quite difficult. Its behaviour differs significantly from ordinary portland cements. The actual model is not fully adequate for this sort of cement mixtures. Further sensitivity analyses of the constitutive model with a variety of different concretes can help to better understand this chemical aspect.

Bibliography

Lochner, F. (1984). Chemie des zements und der hydratationsprodukte. In *Zement-Taschenbuch*.

Appendix A

Results of the Numerical Simulation

The following pages show the results of the numerical simulation gy graphs. The most important and significant figures were already printed in a smaller scale in the previous chapters.

The definition of the shortcuts will be repeated as:

- MKA is the name of the concrete with high cracking sensitivity.
- MKL is the name of the concrete with low cracking sensitivity.
- Wall- centre means in the centre of the one meter thick wall, ($x = 0.50m$).
- Wall- eighth means in the eighth of the one meter thick wall, ($x = 0.12m$).
- Wall- surface means in the surface of the one meter thick wall, ($x = 0.00m$).
- RETA is the retardation time in hours [h]of the maxwell chain .
- ELAS the elasticity modulus constant [-] of the maxwell chain.
- Negative stresses are compressive stresses.
- Positive stresses are tensile stresses.

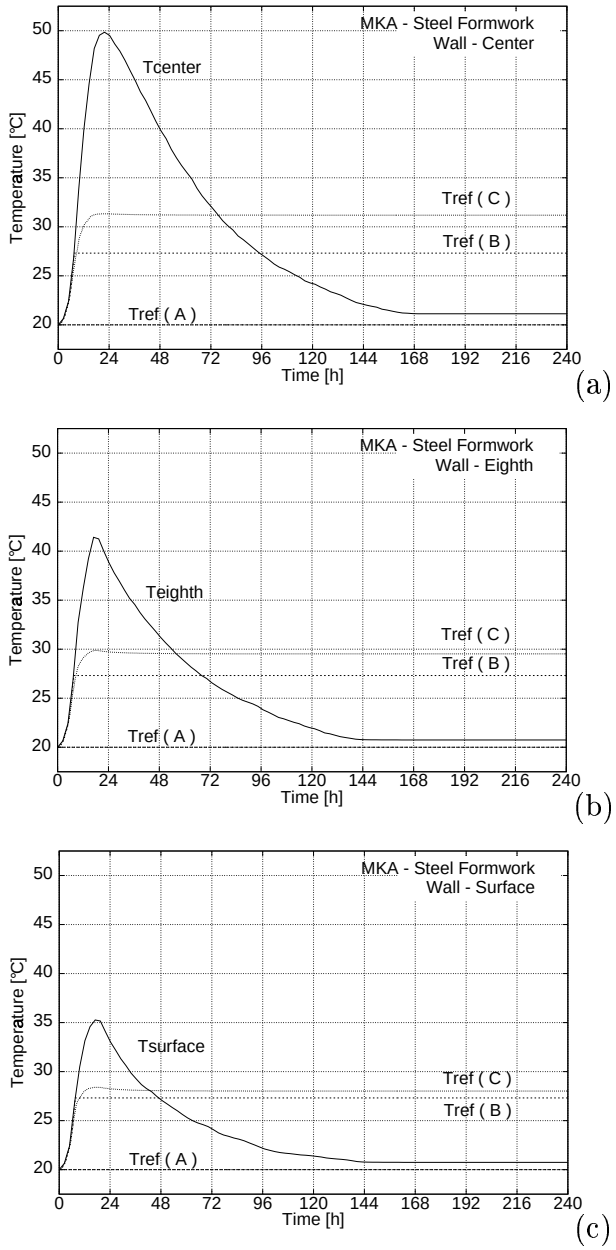

Figure A.1: MKA - Steel Formwork - Input Temperature

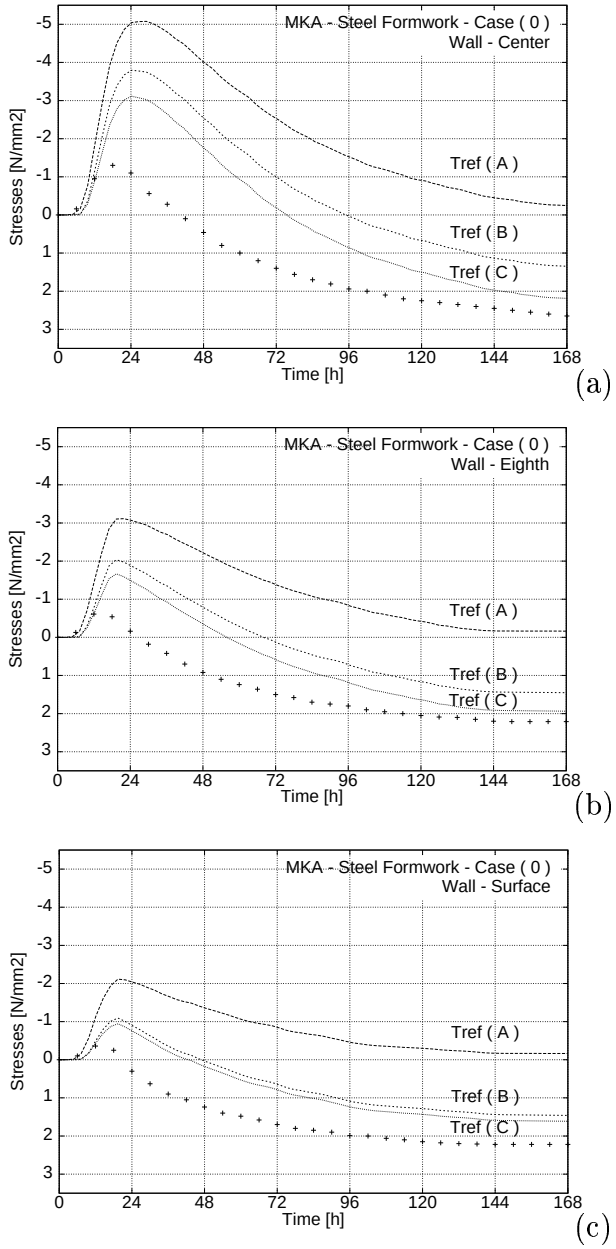

Figure A.2: MKA - Steel Formwork - Case (0)

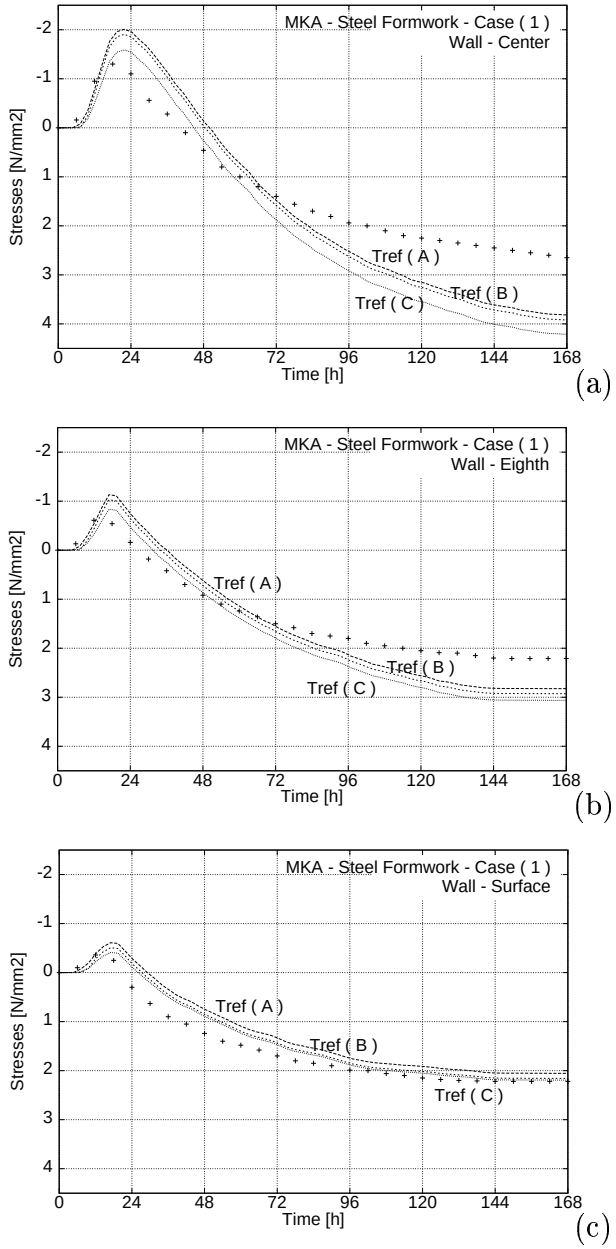

Figure A.3: MKA - Steel Formwork - Case (1)

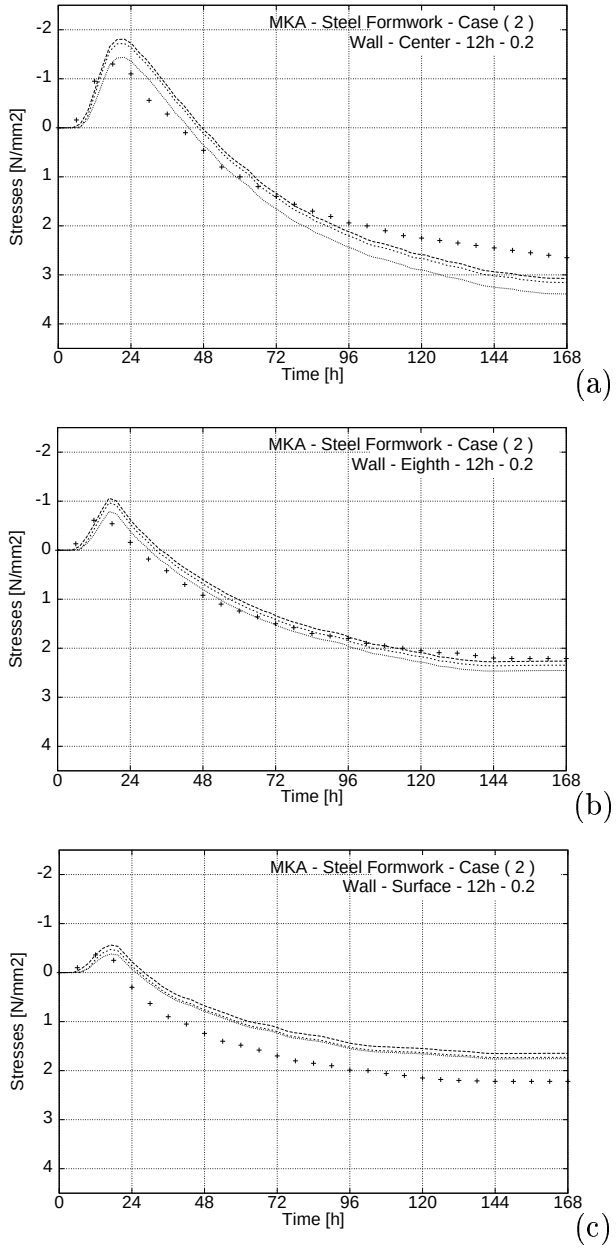

Figure A.4: MKA - Steel Formwork - Case (2)

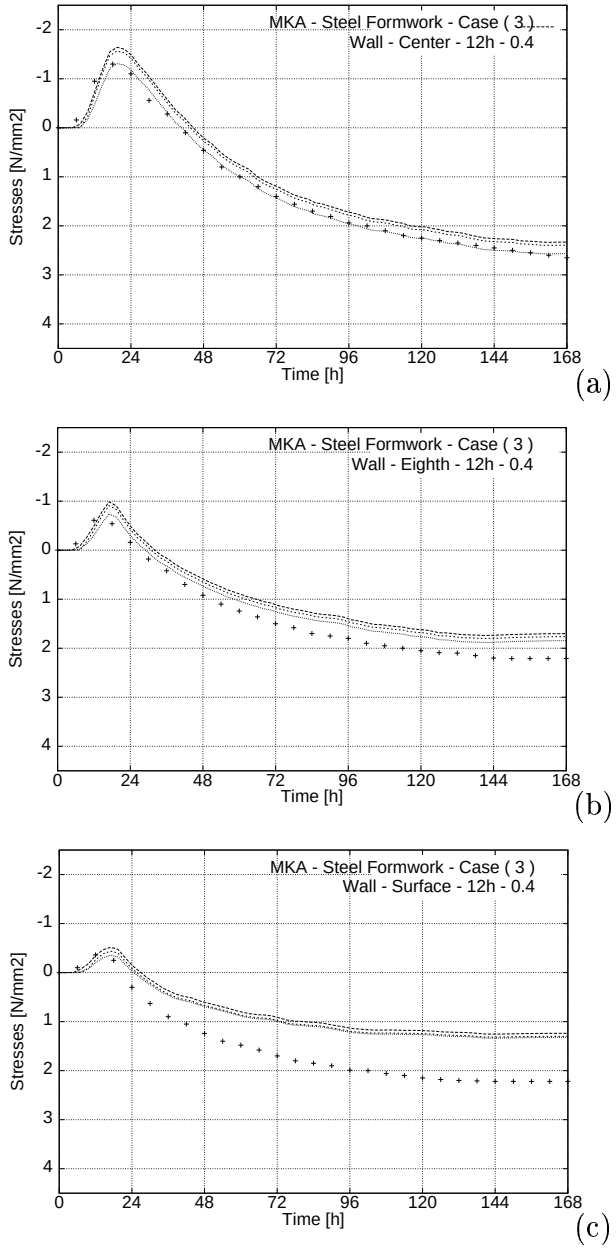

Figure A.5: MKA - Steel Formwork - Case (3)

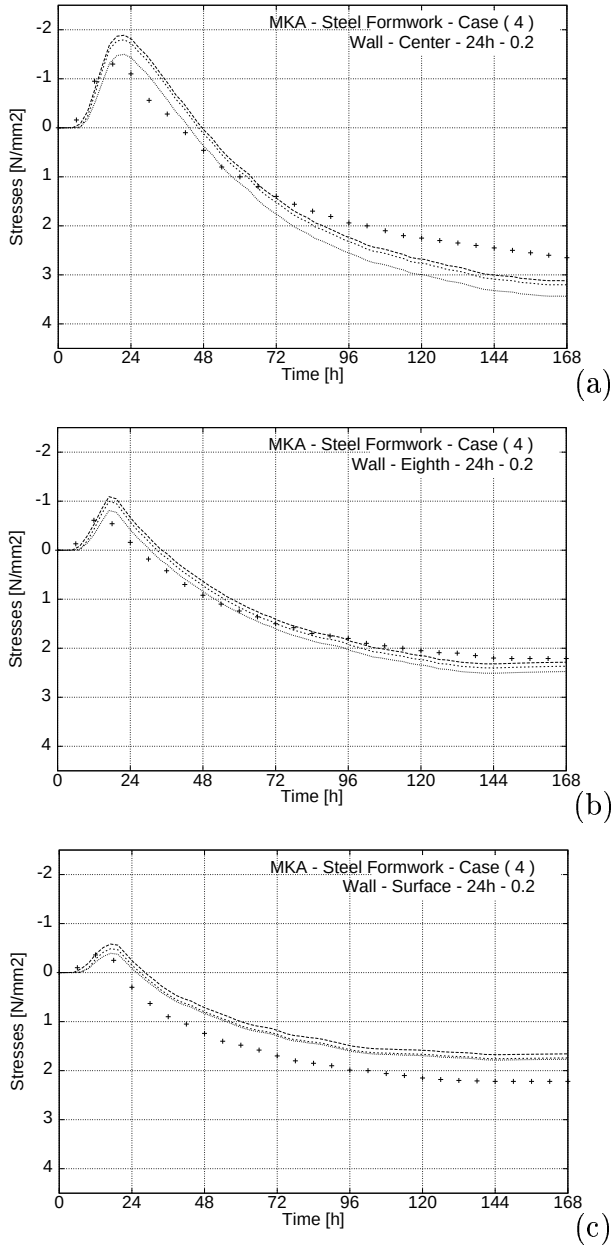

Figure A.6: MKA - Steel Formwork - Case (4)

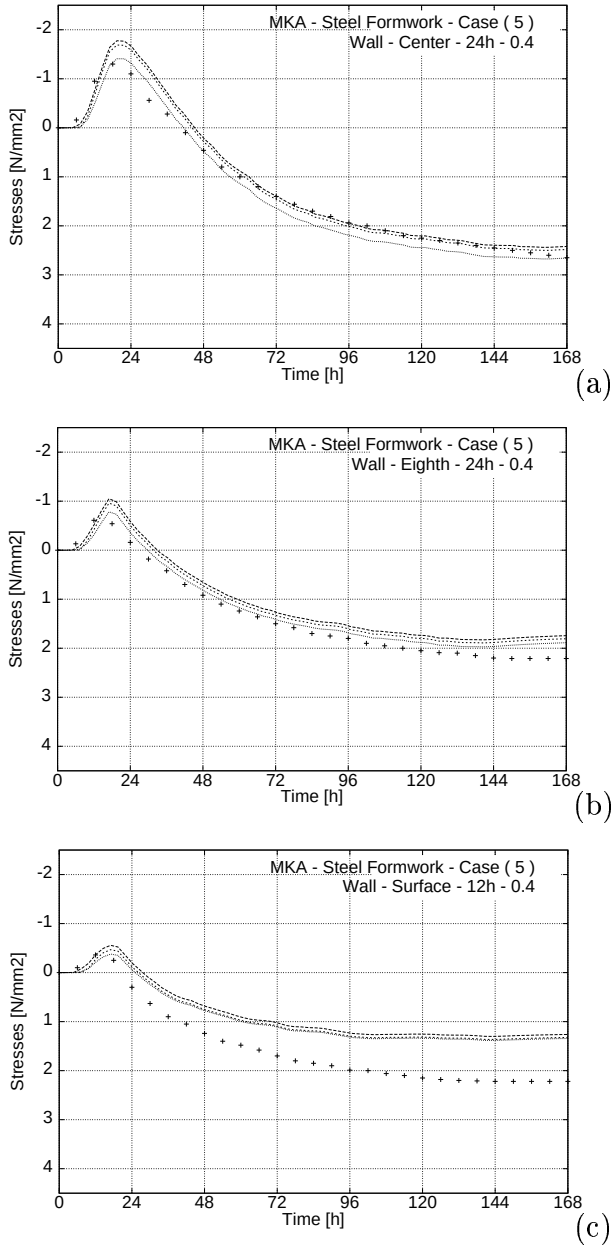

Figure A.7: MKA - Steel Formwork - Case (5)

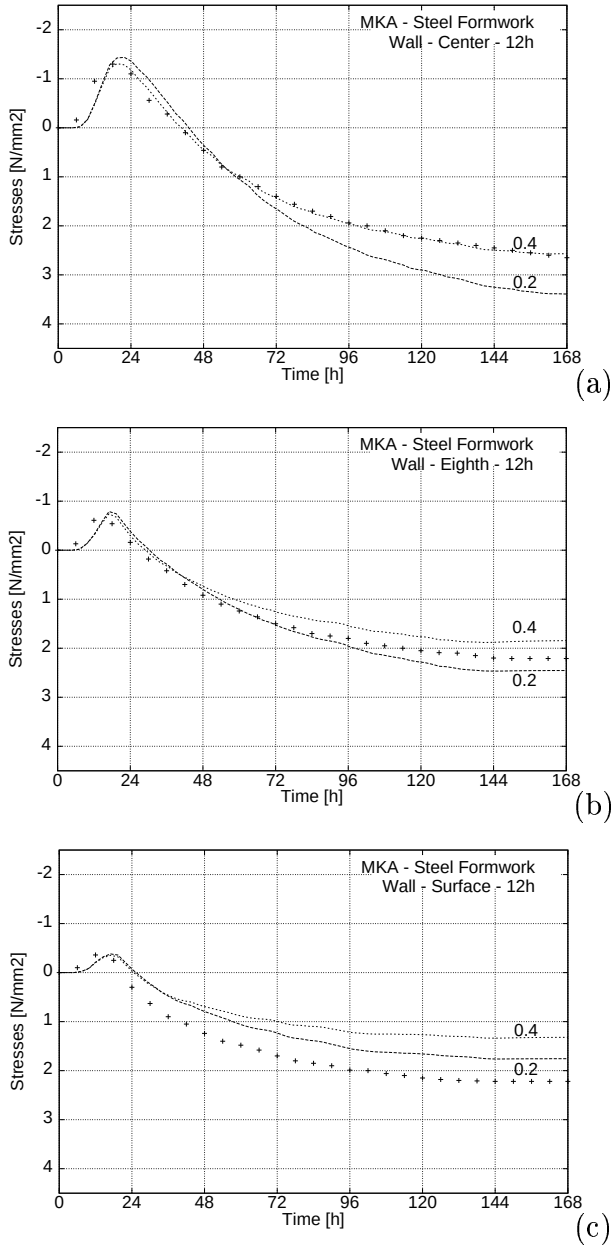

Figure A.8: MKA - Steel Formwork - Case (2) and (3)

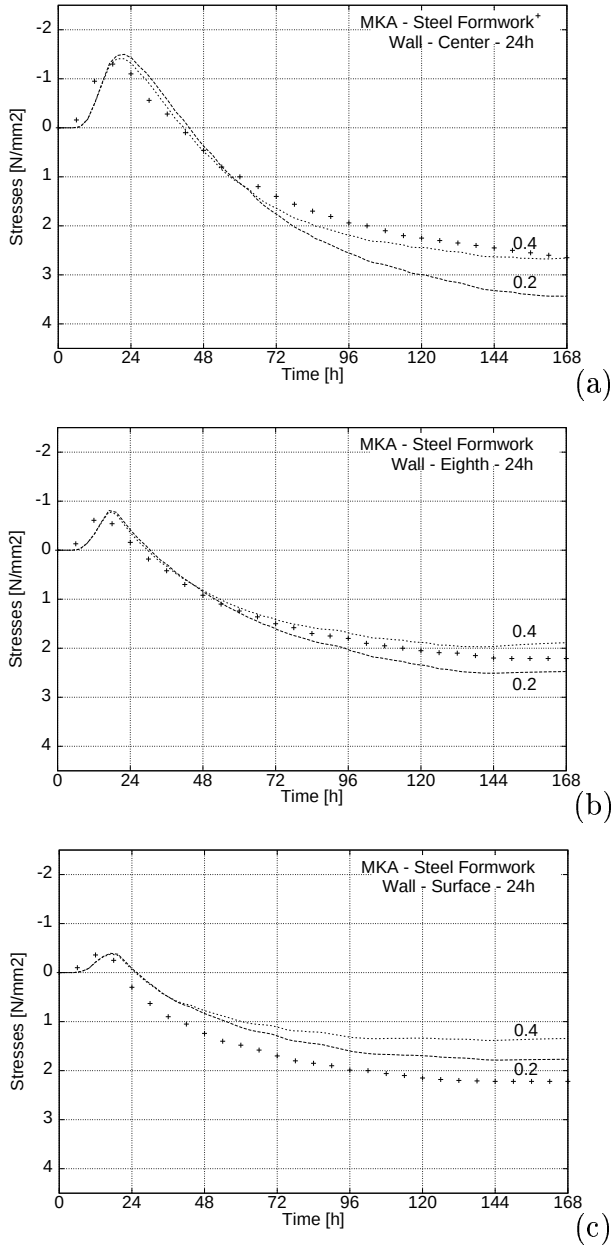

Figure A.9: MKA - Steel Formwork - Case (4) and (5)

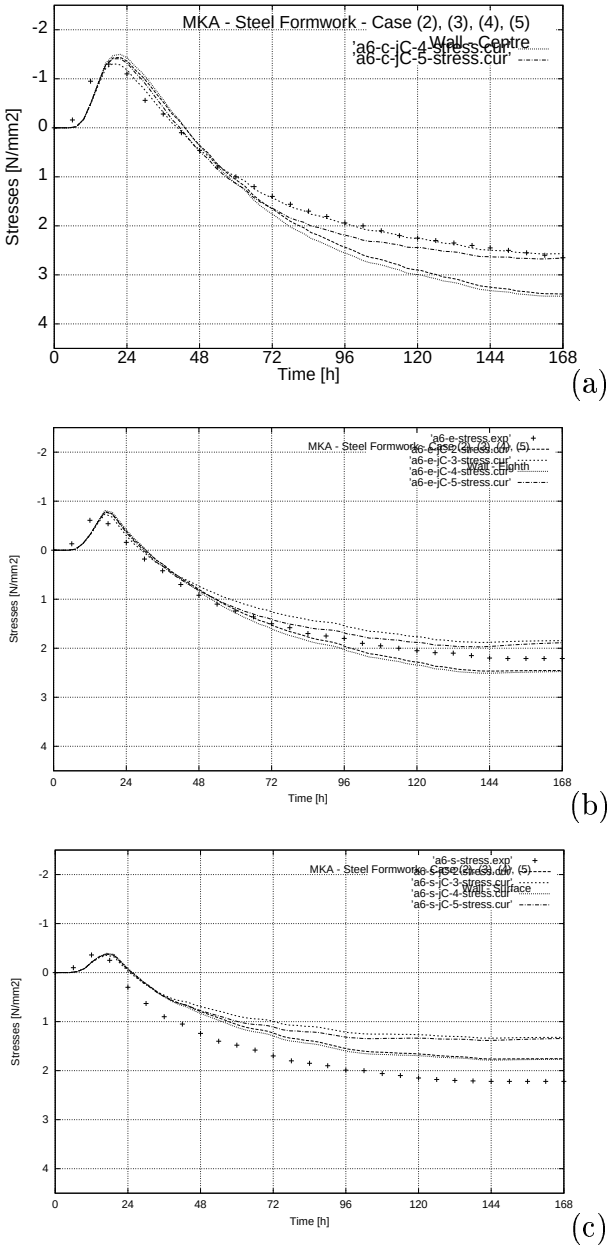

Figure A.10: MKA - Steel Formwork - Case (2),(3),(4) and (5)

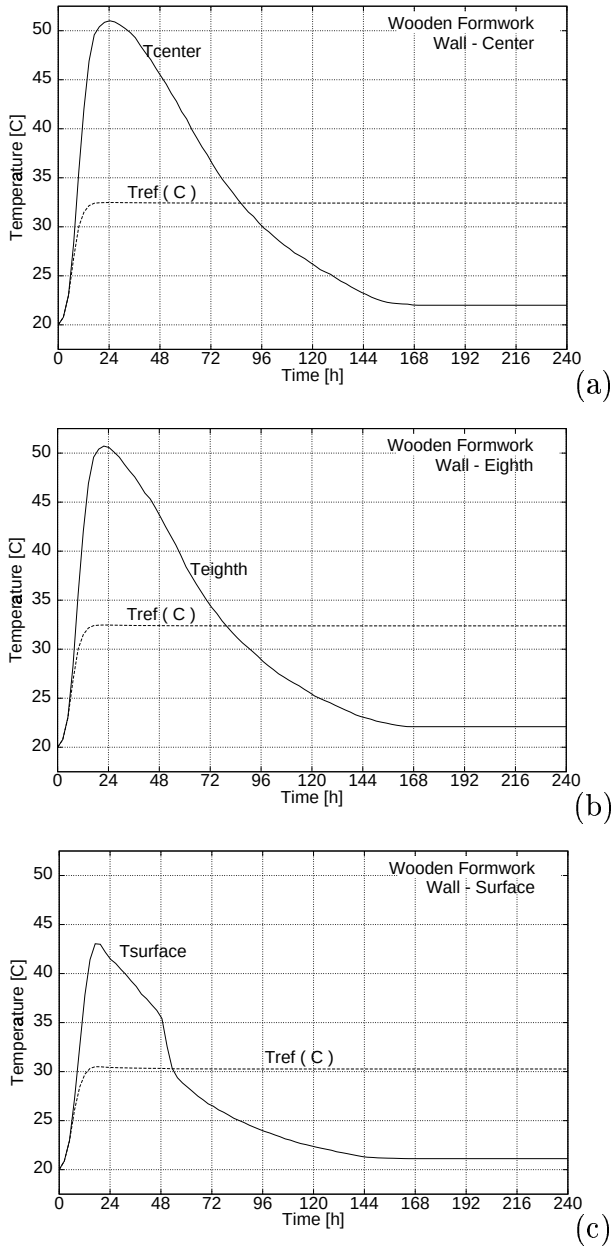

Figure A.11: MKA - Wooden Formwork - Input Temperature

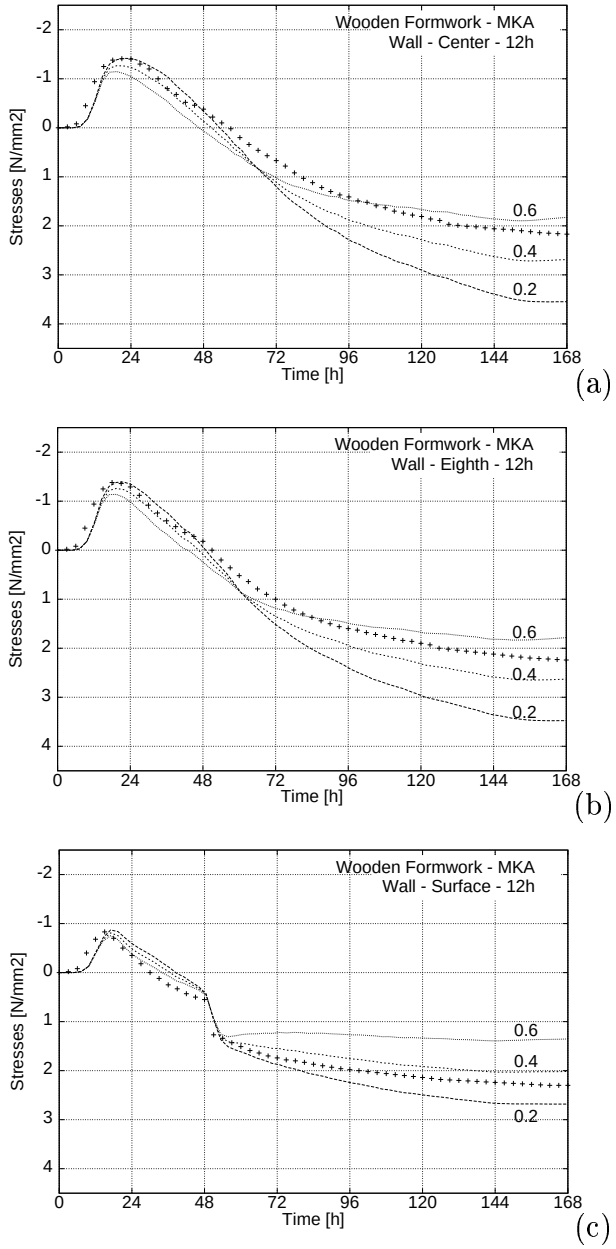

Figure A.12: MKA - Wooden Formwork - Case (2) and (3)

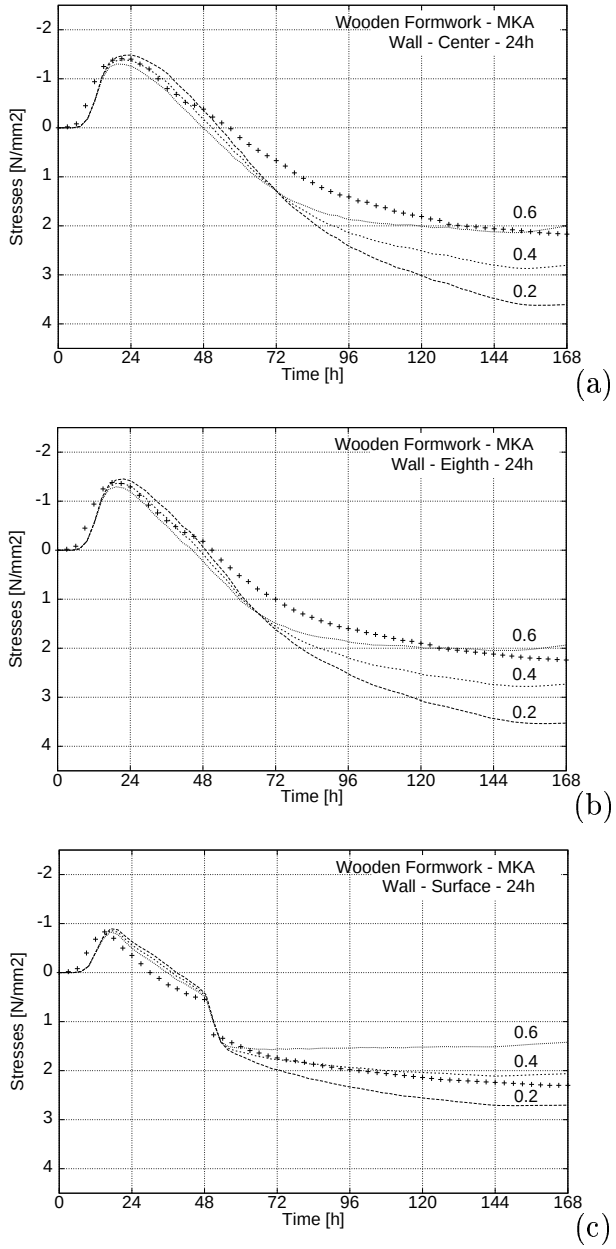

Figure A.13: MKA - Wooden Formwork - Case (4) and (5)

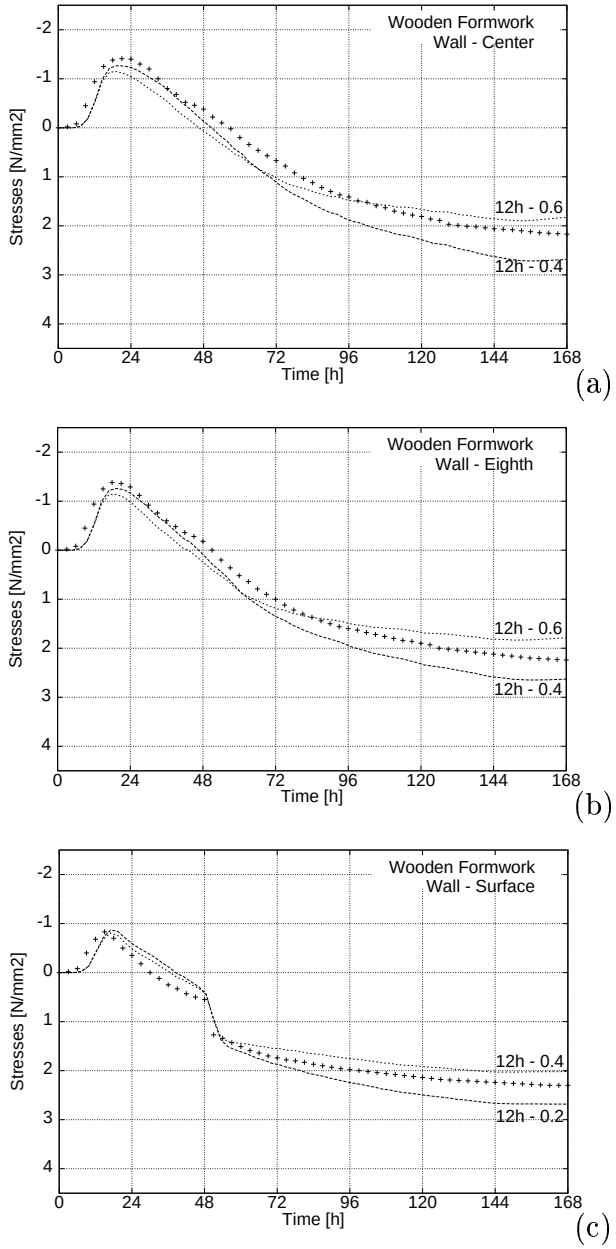

Figure A.14: MKA - Wooden Formwork - Case (2), (3) and (6)

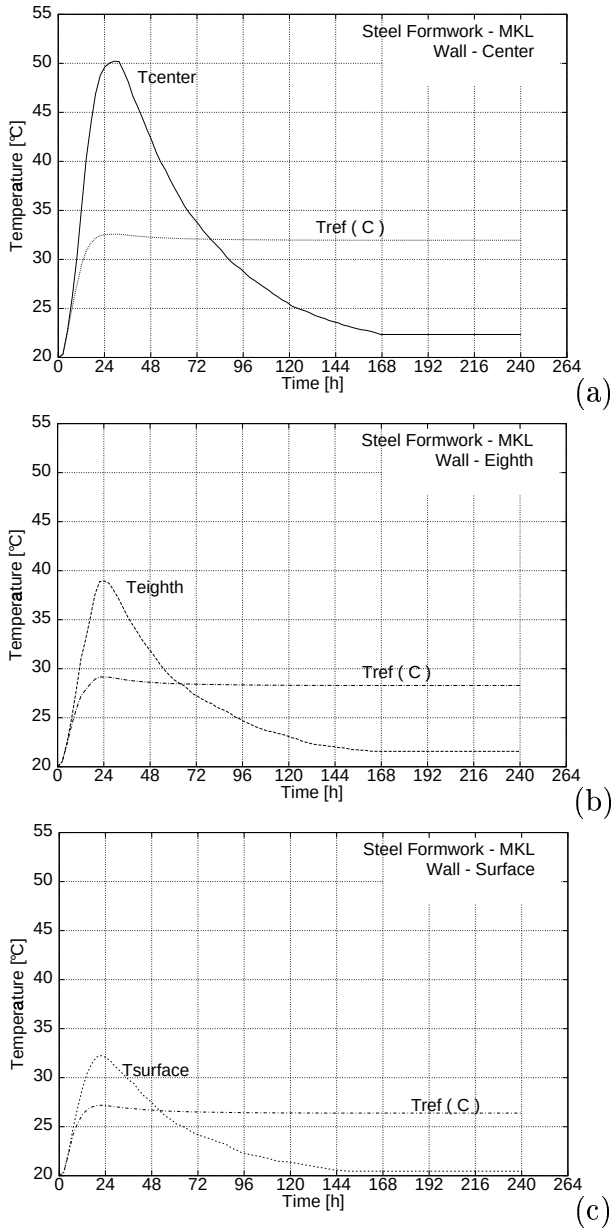

Figure A.15: MKL - Steel Formwork - Input Temperature

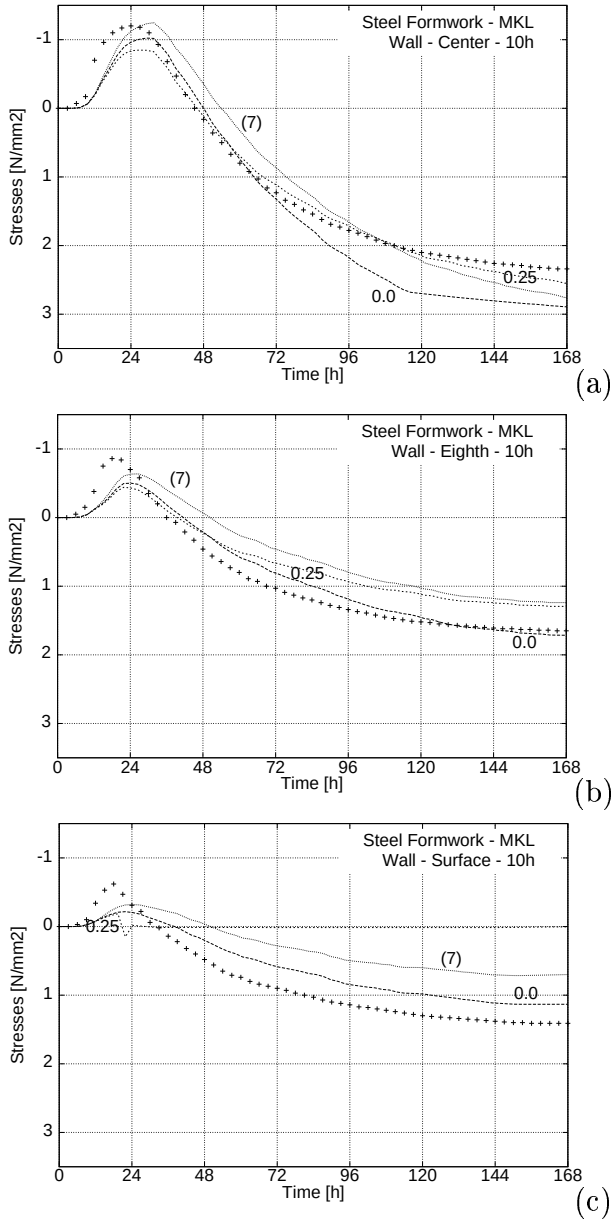

Figure A.16: MKL - Steel Formwork - Case (1), (2) and (7)